Physics – Uspekhi **63** (9) 907 – 928 (2020)

REVIEWS OF TOPICAL PROBLEMS PACS numbers: 06.20.Jr, **07.85. – m**, 61.05.cp, **61.50. – f**

Precise determination of crystal lattice parameters

V V Lider

DOI: https://doi.org/10.3367/UFNe.2019.07.038599

Contents

Abstract. Precision X-ray methods for absolute and relative determination of crystal lattice parameters (interplanar distances) are described and compared, including the X-ray divergent-beam (Kossel) technique, the Bond method, the Renninger method, the back reflection method, the interference method, and the method of standards. It is shown that for most of the considered methods, a relative accuracy of $\sim 10^{-5}-10^{-6}$ for determining the lattice parameters is usually achievable, with the last two methods giving a much greater accuracy, at the level of $\sim 10^{-8}-10^{-9}$.

Keywords: X-ray radiation, diffraction, Bragg angle, crystal lattice parameter, interplane distance

1. Introduction

A lattice parameter can be used to characterize the quality of single crystals if it is measured with a high enough accuracy. A lattice parameter is very sensitive to inhomogeneities, nonstoichiometry, internal or external deformations, impurities, radiation damages, phase transitions, etc.

The inhomogeneous distribution of structural defects and the deviation from stoichiometry can reduce the operation characteristics of semiconductor or optical crystals. In most cases, variations in the crystal composition admissible in practice are very small and are difficult to observe and, moreover, to study by modern chemical and physicochemical methods. However, such studies are possible with the help of invasive X-ray diffraction methods, which are sensitive to relative variations in the interplane distance down to $\Delta d/d \sim 10^{-8}$, corresponding to variations in the composition at the level of $10^{-7}-10^{-8}$ atomic fractions.

The starting point for measuring lattice parameters by X-ray diffraction methods and estimating their accuracy is the Wolf–Bragg law describing the relation between diffraction conditions (the Bragg angle θ and the wavelength λ) and lattice parameters

$$n\lambda = 2d\sin\theta\,. \tag{1}$$

Here, d is the interplane distance depending on the dimensions of the unit cell along three coordinate axes specified by vectors **a**, **b**, and **c**, angles α, β, and γ between these axes, and reflection order n. Therefore, the determination of crystal-lattice parameters involves the measurement of the Bragg angle, more precisely, angular distances between certain features of a diffraction pattern (diffraction maxima or minima, their intersections, etc.)

Crystal-lattice parameters (interplane distances) can be determined by many precision methods. They can all be divided into two groups. The first includes methods in which the interplane distance is determined directly by measuring angular distances. If a priori data on the structure of a crystal under study (for example, angles between crystallographic planes) are known, the lattice parameter can be easily determined from the interplane distance obtained.

The second group includes methods for which the measured angular distances depend on the interplane distances of two or more reflecting planes and the angles between them and can directly give information about the lattice parameter (or parameters).

Measurements of lattice parameters can be divided into absolute measurements, in which the parameters are determined under certain conditions of the environment, and

V V Lider Federal Scientific Research Center
"Crystallography and Photonics",
Shubnikov Institute for Crystallography, Russian Academy of Sciences,
Leninskii prosp. 59, 119333 Moscow, Russian Federation
E-mail: lider@ns.crys.ras.ru, vallider@yandex.ru

Received 14 May 2019, revised 1 July 2019
Uspekhi Fizicheskikh Nauk **190** (9) 971 – 994 (2020)
Translated by M N Sapozhnikov

relative measurements, in which small variations in the lattice parameters are observed compared to a reference crystal or another region of the sample under study. These variations can be caused by temperature, pressure, electric-field, mechanical-stress, etc. variations or by local differences in the unit cell size caused by point defects, deviations from the exact stoichiometry, radiation damage, or other factors.

Absolute methods can be characterized by the accuracy δd determined as the difference between measured and real (unknown) interplane distances or, more often, by the relative accuracy $\delta d/d$ defined by the expression obtained by differentiating Bragg formula (1)

$$\frac{\delta d}{d} = \frac{\delta\lambda}{\lambda} - \cot\theta\delta\theta\,, \tag{2}$$

where $\delta\lambda/\lambda$ is the relative uncertainty in the wavelength and $\delta\theta$ is the error in the Bragg-angle measurement.

A similar criterion used to characterize relative methods may be *precision*. Usually, a measurement is called precise if it is performed with a very high accuracy, i.e., with a record small error. The precision is the degree of mutual closeness of independent results of measurements obtained under particular conditions which are independent of the previous results of measurements of the same or a similar object. The precision depends only on random errors and is not related to the real or found value of the quantity being measured. The precision degree is usually expressed in terms of the inaccuracy and is calculated as the standard deviation of the results of measurements. The relative precision of determining lattice parameters can be written in the form

$$\frac{\sigma(d)}{d} = \cot\theta\,\sigma(\theta)\,, \tag{3}$$

where $\sigma(\theta)$ is the standard deviation of the measured Bragg angle.

Another mathematical criterion is the *sensitivity*, defined by the ratio $\delta\theta/\delta d$, i.e., a change in the Bragg angle caused by changing the interplane distance in a crystal.

However, one should not confuse the terms 'precision' and 'accuracy.'

The *accuracy* is the degree of closeness of the result of measurements to the real value of the quantity being measured. The results of measurements can be precise but not accurate (incorrect) [1]. For example, the accuracy of measuring lattice parameters depends on the relative accuracy of the radiation wavelength used (see expression (2)) and systematic errors caused by the inaccuracy of the adjustment of the experimental equipment, the angular and spectral divergence of an X-ray beam, etc.

Lattice parameters can be measured with powder samples and single crystals. At the first stage of the development of X-ray diffraction methods, the highest accuracy was achieved with powder samples, which were more simply obtained and adjusted. Single crystals were considered more convenient only for systems with a lower symmetry. In the last 60 years, many X-ray diffraction methods for studying single crystals have been developed which provide very high precision and accuracy in the investigation of various specific features inherent only in single crystals (the presence of structural defects and homogeneity degree). These methods are described in reviews [2–4] and monograph [5].

However, the last review [4] was published already more than a decade ago. The aim of our review is to describe X-ray diffraction methods for measuring parameters of the unit cell of single crystals and to present new trends in their development.

2. Kossel projection method

2.1 Obtaining Kossel projections

If a spherical monochromatic X-ray wave propagates in a single crystal, the geometrical place of diffracted beams will be circular conical surfaces with a cone half-angle of $90^\circ - \theta_{hkl}$ and axes perpendicular to the corresponding reflecting planes with Miller indices h, k, l. The intersections of cones with a recording screen or a photographic film give the so-called Kossel lines, the method for obtaining them being called the Kossel method. In this case, the crystal remains stationary and diffraction conditions are fulfilled simultaneously for more than one set of crystallographic planes. Strictly speaking, the Kossel method is one in which a spherical-wave source is located under the crystal surface. If the source is located on the crystal surface (or directly over the surface), the method is called the pseudo-Kossel method, and when the source is located at a distance from the crystal surface, the method is called the X-ray divergent beam (XDB) method. Each of these methods has its own features and application areas. In the discussion of characteristics of these methods, we will call them for simplicity the 'Kossel projection method.'

The fundamental principles and features of formation of Kossel lines are considered in papers [6–13], and the possibilities of using Kossel projections are discussed in [14–17].

Thus, if divergent X-ray monochromatic radiation from a point source S is incident on a single crystal (Fig. 1), then a system of crystallographic planes (hkl) with a nonzero structural factor will reflect rays incident on these planes at the angle θ determined by the Bragg equation. Such beams are the generatrices of a circular cone (Kossel cone) whose axis is parallel to the normal to the given system of reflecting planes.

Depending on the relation between the Bragg angle θ and the angle β between the reflecting plane and photographic film (plate), the Kossel line can be a circle ($\beta = 0$, Fig. 1a), an ellipse ($\beta < \theta$), a parabola ($\beta = \theta$), or a hyperbola ($\beta > \theta$, Fig. 1b).

Besides the reflection cone formed by diffracted beams, an absorption cone appears which is formed by the directions of primary beams in the reflection position. This is a cone of beams with the intensity reduced due to energy 'transfer' into the diffracted beams. These two cones correspond to the

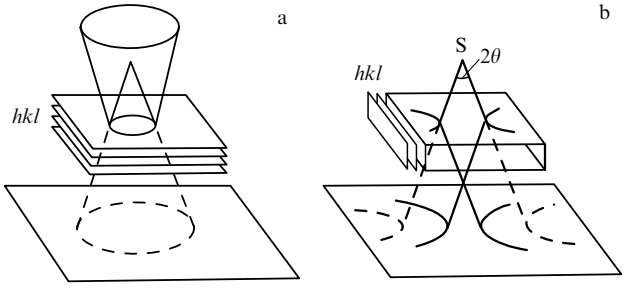

Figure 1. Diagrams of XDB diffraction. (a) Diffraction in transmission and reflection ($\beta = 0$); (b) formation of the intensity deficiency and excess lines ($\beta = \pi/2$).

intensity excess line (solid curves in Fig. 1) and the intensity deficiency line (dashed curves).

The effect was first discovered by Walter Kossel and his colleagues in 1934 [6] during the electron–beam bombardment of a copper single crystal. Soon after that, Borrmann, an assistant at Kossel's laboratory, successfully implemented the method by using an X-ray tube [18, 19]. Kossel projections were also obtained using X-ray tubes in papers [10, 20, 21]. However, the use of a standard X-ray tube does not provide a good locality of studies and is time consuming.

The creator of the X-ray microanalyzer (XMA), R Castaing, [22] was the first to pay attention to the possibility of using it to obtain Kossel diagrams [23]. The modern XMA 'descendant,' the scanning electron microscope (SEM), can be applied to study microstructures and can accommodate additional devices (including devices for heating and deformation). Kossel projections with a spatial resolution of a few micrometers can be used to studying the inhomogeneity of crystals and individual grains in polycrystalline materials. The introduction of XMAs and SEMs into everyday scientific studies resulted in a drastic increase in the applications of Kossel projection methods for investigations of the real structure of crystals in the 1960s and 1970s [12, 24]. For example, electron–beam instruments were used to obtain diffractograms by the Kossel [25–29], pseudo-Kossel [30, 31], and XDB [32–35] methods.

Note that, unlike the XDB method, the pseudo-Kossel method preserves the good locality of the Kossel method: a layer of any material deposited on a sample surface becomes an emitting element. Compared to the Kossel technique, the pseudo-Kossel and XDB methods offer additional advantages allowing investigations of nonconducting and semiconductor samples independently of their electric and thermal conductivity, crystals not containing chemical elements emitting intense lines of the characteristic spectrum, and crystals 'sensitive' to electron irradiation. Because an electron beam is incident on a target rather than directly on a sample, the sample is not heated, and an electric charge is absent near its surface.

An important step was the replacement of the X-ray film by a CCD camera [36], because the digital recording opens the possibility of the automatic analysis of Kossel projections [35, 37]. An SEM with a CCD camera is especially promising in this respect, because it is an easily accessible laboratory instrument, and Kossel diagrams can be processed at once after their recording [27, 38].

It was pointed out in [10, 31, 39] that the line contrast in the Kossel diffraction in transmission strongly depends on the quality of the crystal under study (Fig. 2). In a perfect crystal or one with large structural distortions, Kossel lines are not observed, as a rule, which is understandable: because of a large mismatch between different parts of the crystal, its diffraction reflection curve (DRC) broadens so that, for the high background intensity typical of the Kossel method, the line becomes invisible. For a perfect crystal, the picture is the other way around: the DRC width is now determined by the dynamic X-ray scattering theory and is, as a rule, a few seconds of arc. In this case, the visibility of Kossel lines corresponding to weak reflections can be suppressed by the background, which is mainly determined by bremsstrahlung radiation upon excitation of the characteristic spectrum by accelerated electrons.

In the case of the Kossel recording in reflection, the Kossel line intensity will decrease with distance from a point radiation source proportionally to this distance, whereas the background intensity is proportional to its square [8, 40]. Therefore, the Kossel diagram contrast should improve with increasing source–detector distance [24]. When an X-ray tube or electron–bean instruments are used, this increase in the distance inevitably leads to an increase in the exposure time, which is not always admissible. This limitation can be removed by increasing the X-ray flux density in a focused or collimated X-ray beam exciting in a sample or a target only characteristic fluorescence. The realization of these possibilities using a polycapillary focusing lens [41, 42] and synchrotron radiation (SR) [43] together with a CCD detector attracted new interest in the Kossel projection method in the 1990s.

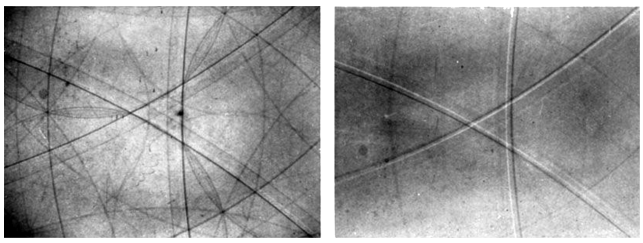

Figure 2. Kossel projections obtained from diamond crystals of different qualities (right projection corresponds to the less perfect crystal) illuminated by radiation from an X-ray tube with a copper anode (lines forming a 'triangle' at the center of the projections correspond to {111} reflections) [10].

According to [44, 45], the use of a polycapillary lens can provide a two-order magnitude increase in the radiation intensity by focusing X-rays in a broader solid angle.

When Kossel diffraction is excited by a focused or collimated SR beam [46], it follows from pioneering paper [47] that the decrease in the irradiated sample region to 1 μm^2 does not contradict the short exposure time, which can be shortened here to a few minutes or even seconds. As a result, papers were published in which fine-crystalline objects were studied (for example, deformation inside an individual grain of a polycrystal was investigated in [48] and mosaic quasicrystals were studied in [49]). In paper [50], the fluorescence yield of a chemical element contained in the sample was increased by using a monochromator mounted between the SR source and sample, which was also used for selective excitation of one of the elements by selecting the X-ray beam energy close to the absorption edge of the chosen element.

It is clear that SR use in the Kossel method probably has a single restriction: the absence of a 'suitable' chemical element in the sample under study. Because of this, the authors of [51] were forced to study diamond by the pseudo-Kossel method by mounting a niobium plate in the SR beam close to the sample.

2.2 Determining single-crystal lattice parameters

In 1947, Lonsdale [52] showed for the first time in her classical paper [10] via the example of cubic syngony crystals that the distance between Kossel lines or their intersection points are sensitive to variations in the crystal lattice parameter (Fig. 3).

The high accuracy of measuring crystal-lattice parameters ($\Delta a/a \sim 10^{-5}$) follows from the accurately known wavelength of characteristic X-ray radiation ($\delta\lambda/\lambda = 10^{-6}$ [53, 54]), large Bragg angles (i.e., a small Kossel cone angle), and diffraction Kossel lines, whose positions can be accurately measured. Note that, to obtain accurate values of the lattice

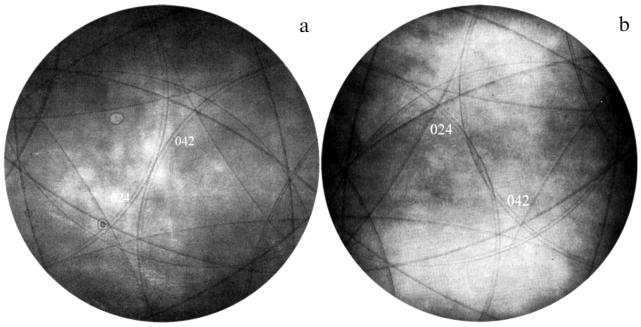

Figure 3. Diffraction patterns obtained by the Kossel method from a Cu single crystal: (a) a contact of the lines corresponding to the (042) and (024) reflections is observed at $T = 262\,^{\circ}\mathrm{C}$ and (b) these lines overlap at $T = 363\,^{\circ}\mathrm{C}$ [16].

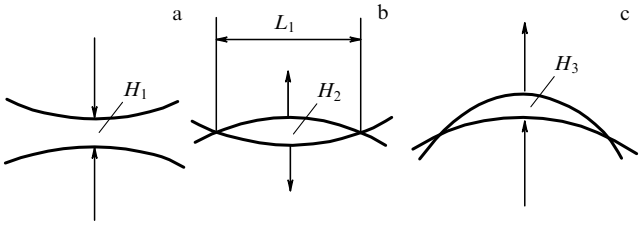

Figure 4. Possible configurations of 'deficiency' Kossel lines used for precision measurements of crystal lattice parameters [14].

parameter, the sample temperature should be maintained constant during measurements [16, 48].

The measurement of lattice parameters is usually started with the indexation of Kossel projections. For this purpose, as a rule, a stereographic projection is used, which reflects the diffraction pattern in the whole half-space over (under) the crystal surface and is simple to construct. The gnomonic projection should be used to map the diffraction pattern of a small part of a stereographic projection chosen for further studies [34].

The construction of projections 'manually' is a tedious, time-consuming process. Algorithms and computer software for the geometrical construction of projections and indexation of Kossel diagrams are described in many papers (for example, [31, 34, 48, 55–60]).

Because the mutual location of lines obtained from an undeformed crystal obeys strict symmetry laws, the precision determination of crystal-lattice parameters can be reduced to the measurement of distances between lines of their intersection points in Kossel diagrams (H_1, H_2, H_3, and L_1 in Fig. 4, respectively). The arrows in Fig. 4 show the directions of Kossel line displacements upon increasing the lattice parameter. Obviously, the configuration in Fig. 4c (convex-concave lens) should be less sensitive to the change in the lattice parameter than that in Fig. 4a (double-concave lens) or in Fig. 4b (double-convex lens).

The accuracy of measuring the lattice parameter by methods illustrated in Fig. 4 is given by the expression

$$\frac{\delta a}{a} \approx (\tan\theta_1 \pm \tan\theta_2)^{-1}\,\frac{\delta H_i}{Z'}\,, \tag{4}$$

where θ_1 and θ_2 are Bragg angles of reflections from crystallographic planes with Miller indices $h_1k_1l_1$ and $h_2k_2l_2$, respectively, forming a pair of Kossel lines; δH_i is the accuracy of measuring distances H_1, H_2, and H_3; Z' is the distance from the radiation source to the 'lens' center; and the signs + and − correspond to cases a (b) and c in Fig. 4, respectively. Assuming that the precision criterion of the method is the condition $\delta a/a \leqslant 10^{-5}$, we see that, to fulfil it, even for the quite high accuracy of measuring the distance H_i ($\delta H_i/Z' \approx 10^{-4}$), it is necessary to select Kossel cones with small cone angles for which $\tan\theta_1 + \tan\theta_2 \gg 1$. However, in this case (i.e., for large Bragg angles), Kossel lines can be blurred and 'weakly contrasting' due to the high dispersion of the spectral line used, which will inevitably reduce the accuracy of their localization. The geometry of the lens-like intersection of Kossel lines (Fig. 4b) shows that the distance L_1 should be more sensitive to changes in the lattice parameter than the distance H. Then, the parameter a is determined by the expression [61–63]

$$a = K\sec\left(\frac{\Gamma}{2}\right), \tag{5}$$

$$K^2 = \left(\frac{\lambda}{2}\right)^2 \frac{\Sigma_1^2\Sigma_2^2\left[(h_2-h_1)^2 + (k_2-k_1)^2 + (l_2-l_1)^2\right]}{\Sigma_1\Sigma_2 - (h_2h_1 + k_2k_1 + l_2l_1)^2}\,, \tag{6}$$

$$\sec^2\left(\frac{\Gamma}{2}\right) = \frac{4AB}{(A+B)^2 - L^2}\,, \tag{7}$$

where $\Sigma_1^2 = h_1^2 + k_1^2 + l_1^2$, $\Sigma_2^2 = h_2^2 + k_2^2 + l_2^2$, $A^2 = P_1^2 + Z^2$, and $B^2 = P_2^2 + Z^2$, P_1 and P_2 are distances between the center O of the picture and the intersection points of Kossel lines, and Γ is the angle between directions to these points (Fig. 5).

As follows from (5), the accuracy of measuring the lattice parameter is $\delta a/a = (1/2)\tan(\Gamma/2)\,\delta\Gamma$ ($\delta\Gamma$ is the accuracy of measuring the angle Γ). Thus, lens-like configurations with a small angle Γ should be quite sensitive to variations in the lattice parameter.

In the general case, six lattice parameters exist: three linear (a, b, c) and three angular (α, β, γ). If six independent pairs (intersections) of Kossel lines can be measured, then all the lattice parameters can be found from a system of six equations [63].

Note that expressions (5)–(7), generally speaking, allow one to measure precisely the lattice parameter because parameters L, P_1, and P_2 in them can be measured quite accurately on a photographic film (some methods of determining the position of the center of a picture determining the accuracy of measuring P_1 and P_2 are described in

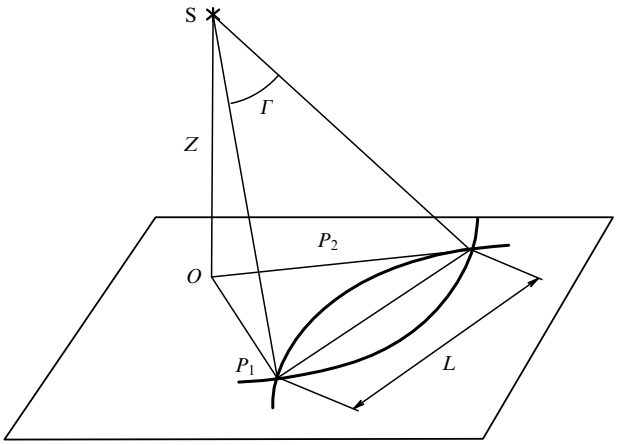

Figure 5. Geometry of the lens-like configuration of Kossel lines [63] (see text).

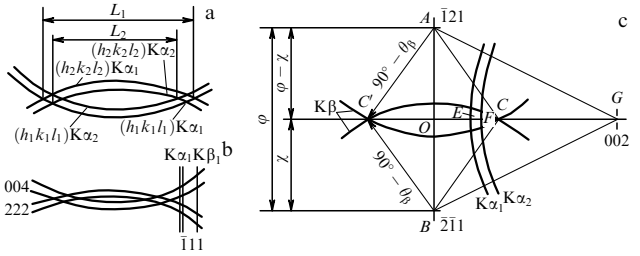

Figure 6. Configuration of Kossel lines used for precision determination of the cubic lattice parameter by measurements on a photographic film [68] (see text).

papers [24, 64–66]). The exception is the distance Z from the source to the film, whose measurement error can considerably reduce the accuracy of determining the lattice parameter. To eliminate this parameter in the general case, it is sufficient to measure distances L, P_1, and P_2 corresponding to two wavelengths (for example, $K\alpha_1$ and $K\alpha_2$ in Fig. 6a [67]). In such a way, the authors of [21] obtained the accuracy of measuring the LiF lattice parameter equal to 8×10^{-6}.

Another way to eliminate the parameter Z is the use of an 'angular reference' — the distance between the spectral lines of the reflection weakly dependent on the lattice parameter. In [40], the lattice parameter of a nickel crystal irradiated by electrons ($\delta a/a$ was about 10^{-5}) was measured using the $K\alpha_1 - K\beta_1$ pair of the (111) reflection as such a reference (Fig. 6b).

The influence of various impurities on the α-Fe crystal lattice parameter [68] was studied using Kossel lines corresponding to the Kα doublet of the (002) reflection as a reference and also as an element, forming together with a part of a 'lens' consisting of the $(\bar{1}21)K\beta_1$ and $(\bar{2}\bar{1}1)K\beta_1$ Kossel lines a spherical isosceles triangle with the height EC (Fig. 6c) very sensitive to variations in the lattice parameter:

$$EC = Z\big[\tan(OC) - \tan(OG - EG)\big]\,. \tag{8}$$

Here, O is the photographic film center, EC is the distance measured on the film, and OC, OG, and EG are angles defined according to the trigonometry of spherical triangles: $\cos(OC) = \sin\theta_{\bar{1}21}/\cos\chi$, $\cos(OG) = 6^{-1/2}/\cos(\varphi - \chi)$, and $EG = 90° - \theta_{002}$.

The quasi-intersections of three Kossel lines at one point can be especially efficiently used for precision measurements of the lattice parameter. The method is based on the choice of suitable reflections for obtaining the triple diffraction pseudo-point and determining the wavelength required to obtain this triple point. Results presented in [10, 20, 34, 69–75] show that this method provides simple and rapid measurements of lattice parameters with an accuracy better than 1×10^{-5}.

Although computer simulations can considerably facilitate the search for 'suitable' intersections and configurations of Kossel lines, they cannot be found for some crystal objects, especially by the Kossel method. For this reason, Morrison developed a method for determining interplane distances by measuring the coordinates of several points belonging to the corresponding Kossel line [63]. The Kossel line equation has the form

$$q_1x + q_2y + q_3Z = (x^2 + y^2 + Z^2)^{1/2}\sin\theta\,, \tag{9}$$

where q_1, q_2, and q_3 are the direction cosines of the Kossel cone axis ($q_1^2 + q_2^2 + q_3^2 = 1$), x and y are Cartesian coordinates on the Kossel diagram (the coordinate origin x_0, y_0 is located at its center), and Z is the distance from a radiation source to the Kossel diagram center. By minimizing variations in the lattice parameter obtained in calculations of several lines, one can determine the distance Z [25], thereby improving the accuracy of the method. Progress in the digital imaging opens up the possibility of simplifying and improving the Kossel projection studies. Such projections can be processed at once after their recording by using appropriate computer software.

The main task at present is to automate a system for determining crystal-lattice parameters as well as possible. In this respect, the KSLStrain software package [76] is a noticeable step to a more complex automated analysis of Kossel diffraction patterns. All the stages of the Kossel diagram interpretation (i.e., the geometrical simulation) are based on a comparison of experimental Kossel lines indicated by markers (p_i) (Fig. 7) (and represented by vectors p_i) with the corresponding lines in simulated schemes. Along with lattice parameters, the crystal orientation, the distance between the sample and detector, and the position of the projection center can be refined.

Lattice parameters can be fitted simultaneously for several models [77]. Some empirical rules for selecting marker positions on Kossel lines are contained in [78]. The results of the program tests are presented in [29, 78]. For example, the accuracy of measurements of lattice parameters using the KSLStrain program was 6×10^{-5} for copper and 2×10^{-5} for germanium [29].

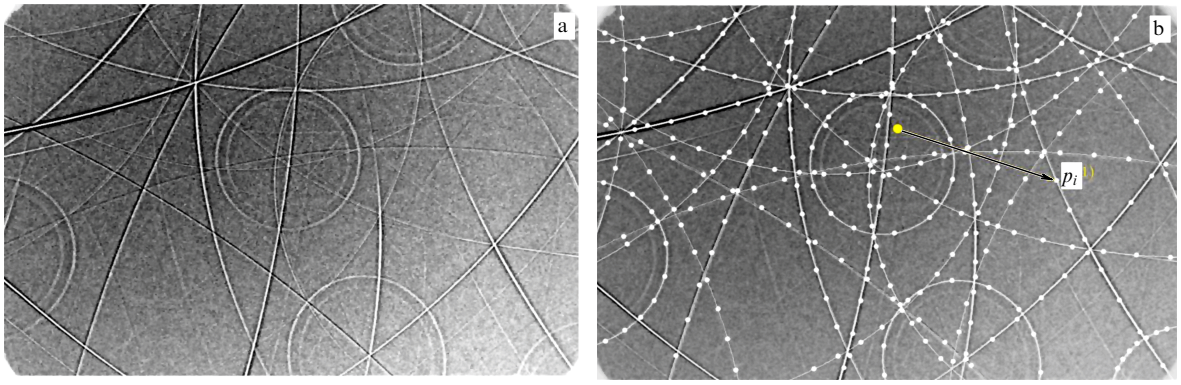

Figure 7. (a) Kossel projection of the CuBeAl alloy. (b) The same projection with markers (white dots) on Kossel lines. The approximate location of the projection center and one of the vectors p_i are shown [77].

2.3 Determining interplane distances

The XDB method in reflection is inferior to the Kossel and pseudo-Kossel methods in its locality, but offers a number of significant advantages, such as a good contrast of Kossel diagrams, the possibility of studying the homogeneous deformation of a crystal, and the determination of parameters for a crystal of the lowest syngony.

But, unlike the Kossel method, in which all the diffraction cones have the same apex, in the XDB method in reflection, diffraction lines are constructed with the participation of imaginary sources (apexes of cones) separated macroscopically in space [13, 79]. In this case, the diffraction line equation on a photographic film will be of the fourth degree rather than the second one [80]:

$$F = (x^2 + y^2)\sin^2\theta - x^2\sin^2\alpha - \cos\theta\sec\alpha\left[(Z_\mathrm{f} + 2Z_\mathrm{s})\sin\theta\cos\alpha\,(x^2 + y^2\sec^2\alpha)^{1/2} + Z_\mathrm{f}x\cos\theta\sin\alpha\right] = 0\,. \quad (10)$$

Here, Z_f and Z_s are distances from the radiation source to the photographic film and sample, respectively, and α is the angle between the crystal surface and reflecting plane.

A new way of simulating diffraction patterns obtained by the XDB method in reflection was proposed in the KOPSKO program [59] for determining the crystallographic structure, orientation, indexation of reflections, and interplane distances in crystals.

The number of XDB studies increased in the 1960s–1970s to a great extent due to the advent of microfocus X-ray tubes, in particular, the Microflex, Rigaki Denki (Japan) device with a changeable capillary anode holder emitting characteristic X-rays from a 10-μm area with a divergence of $\sim 180^\circ$ [81]. Figure 8 shows a Kossel projection typical of the XDB method in reflection.

Imura and his coworkers [81] proposed to measure the interplane distance in crystals from the size of the major axis of a pseudo-ellipse (note that, as follows from (10), the minor axis, unlike the major axis, is not its symmetry axis). But even the use of a brass foil (the picture contained pseudo-ellipses corresponding to the CuK and ZnK spectra) did not allow the authors to avoid the measurement of geometrical parameters Z_f and Z_s, which could not but affect the accuracy of measuring d.

To exclude the geometrical parameters of the survey, the authors of [83] proposed to use a multiple survey with the successive displacement of a photographic film by a strictly fixed distance (Fig. 9a).

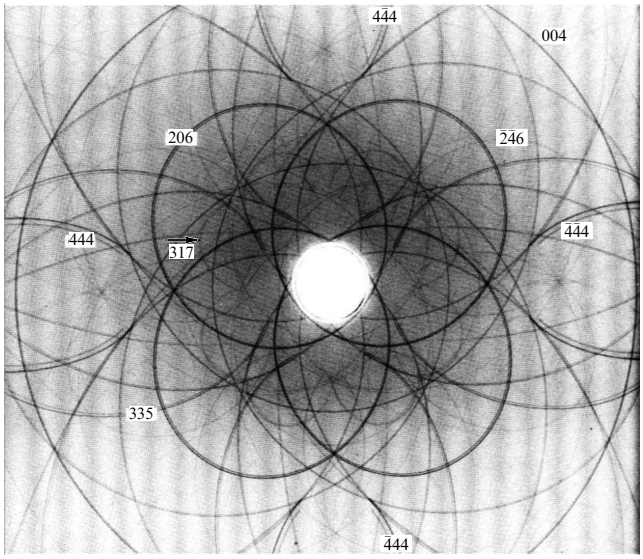

Figure 8. Kossel diagrams obtained by the XDB method in reflection from a Si(001) crystal using CuK radiation [82]. The hole at the image center serves as a 'window' for a capillary holder of the anode of a microfocus X-ray tube.

During such a survey, each system of reflecting planes produces concentric pseudo-ellipses on the photographic film (see Fig. 8), and the interplane distance is determined by the expression

$$d = \frac{\lambda}{2}\sec\left\{0.5\left[\arctan\left(\frac{p}{\Delta Z_{12}}\right) + \arctan\left(\frac{q}{\Delta Z_{12}}\right)\right]\right\}, \quad (11)$$

where p and q are the displacements of the opposite parts of pseudo-ellipses measured along their major axes, and ΔZ_{12} is the reference distance between successive positions *1* and *2* of the film (Fig. 9a). The accuracy of measurements can be considerably increased by increasing the number of exposures [83]. The relative accuracy of determining d depends on the Bragg angle of a reflection and can be $\sim 10^{-4}$ [85]. This accuracy is sufficient in many cases for calculating the deformation tensor.

However, the capillary anode holder in this scheme can screen some beams of the diffraction cone (more exactly, the pseudo-cone) (see Fig. 8). In this case, expression (10) cannot be used. This circumstance considerably restricts the scope of applications of this method. The authors of [83] solved this problem by using two spectral lines for process-

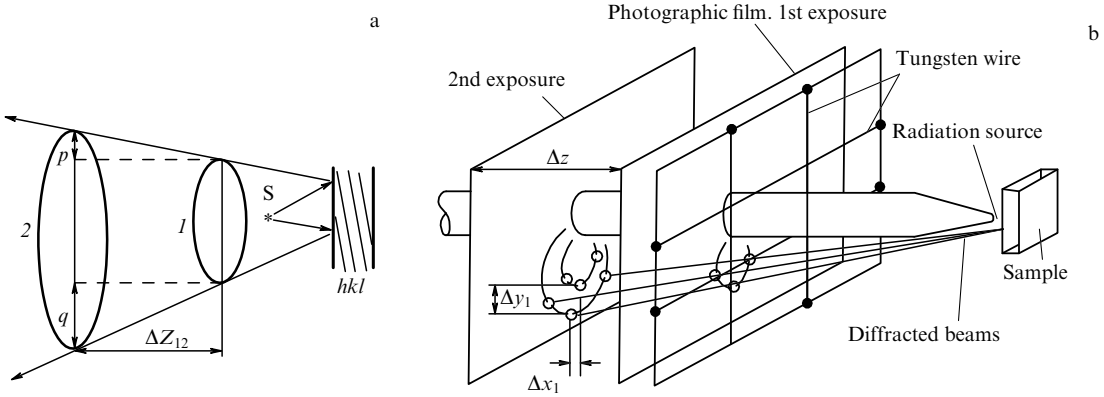

Figure 9. Formation of a diffraction pattern in methods of (a) multiple shooting and (b) beam tracing [84] (see text).

ing 'unfinished' pseudo-ellipses. In this case, the interplane distance can be determined from the expression

$$d = 0.5\left[(\lambda_1^2 + \lambda_2^2)(1 + s^2) + 2\lambda_1\lambda_2 s(1 + s^2)^{1/2}\right]^{1/2}, \qquad s = \frac{\Delta Z_{12}^2 + \Delta_1\Delta_2}{\Delta Z_{12}(\Delta_1 - \Delta_2)}, \tag{12}$$

where Δ_1 and Δ_2 are distances between pseudo-ellipses corresponding to spectral lines with wavelengths λ_1 and λ_2 measured along their common major axis.

Another method of using 'unfinished' lines for studying the anisotropic deformation (we will call it the beam tracing method) was applied in papers [13, 86, 87]. A semitransparent screen representing a metal wire grid was placed in the path of diffracted beams. As a result, breaks appeared in the diffraction lines (Fig. 9b). The diffraction pattern was recorded by successive exposures on the same film displaced by the fixed distance Δz. The coordinates of a line break determine the diffracted beam for which the equality is valid:

$$\sin\theta = n_x s_x + n_y s_y + n_z s_z, \tag{13}$$

where n_x, n_y, n_z and s_x, s_y, s_z are the direction cosines of the normal to the reflection plane and the diffracted beam, respectively. Taking the condition $n_x^2 + n_y^2 + n_z^2 = 1$ into account, the problem of determining the Bragg angle and the direction cosines of the normal is reduced to the experimental determination of the direction cosines of three beams. The direction cosines are calculated from the expressions

$$s_{xi} = \frac{\Delta x_i}{M_i}, \quad s_{yi} = \frac{\Delta y_i}{M_i}, \quad s_{zi} = \frac{\Delta z}{M_i}, \qquad M_i = (\Delta x_i^2 + \Delta y_i^2 + \Delta z^2)^{1/2}, \tag{14}$$

where Δx_i and Δy_i $(i = 1, 2, 3)$ are the change in the coordinates of breaks in the diffraction line (Fig. 9b).

But because it is difficult to determine the coordinates of line breaks with sufficient accuracy, the relative errors in determining the interplane distance are, as a rule, no better than 10^{-4}. The modification of the method described in [88] will considerably improve, in the opinion of the authors, the accuracy of calculating d.

Let us return to the consideration of the features of a diffraction pseudo-ellipse and the question of why researchers have mainly focused on its major axis (which often cannot even be measured) and 'ignore' the possibility of using the value of the minor axis. The answer is that, unlike the major axis, the minor axis is not the symmetry axis of a pseudo-ellipse, and therefore its localization is complicated by symmetry considerations. Expression (10) shows that an 'ellipse' transforms into a centrically symmetric figure when $Z_f x \cos\theta \sin\alpha = 0$. This equality is fulfilled if $\alpha = 0$ or $Z_f = 0$. The first condition means that reflection planes are parallel to the sample surface and a film, i.e., the pseudo-ellipse, transforms into a circle with radius $(Z_f + 2Z_s)\cot\theta$.

The second condition corresponds to the case when a point radiation source is located at the film level, which in turn is parallel to the sample surface. In this case, the major (a) and minor (b) axes are determined by the expressions

$$a = 2Z_s\left[\cot(\theta - \alpha) + \cot(\theta + \alpha)\right], \tag{15}$$

$$b = 4Z_s \cot\theta \sec\alpha. \tag{16}$$

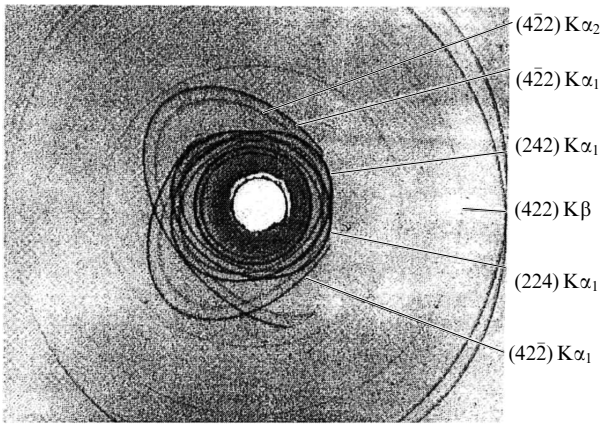

Figure 10. Diffractogram obtained by the XDB method from a Ge(211) crystal for $Z_f = 0$ using CrK radiation [90].

To determine the interplane distance when $\alpha = 0$, it is sufficient to measure the diameters of two diffraction circles, and for $Z_f = 0$, the minor axes of two pseudo-ellipses corresponding to different wavelengths or different reflection orders.

When the condition $\alpha = 0$ is fulfilled, it is possible to measure only one interplane distance, which can be used to determine the cubic-lattice parameter [89]. In the more general case, the diffraction pattern consists of pseudo-ellipses with the same center coinciding with the radiation source. Note that here the screening of diffracted beams is absent and the 'truncated' pseudo-ellipse can be formed only because of the finite size of the sample (Fig. 10).

The relative error of the method is calculated by the expression

$$\frac{\delta d}{d} = \left|\tan\theta_1^2 - \tan\theta_2^2\right| \frac{\delta\sigma}{\sigma}. \tag{17}$$

Here, θ_1 and θ_2 are Bragg angles corresponding to two wavelengths (two reflection orders), and $\delta\sigma/\sigma$ is the relative error of measuring the ratio σ of minor axes of pseudo-ellipses. For example, in determining the germanium lattice parameter for {422} reflections, $\theta_1 \approx 82^\circ$ (CrKα_1), $\theta_2 \approx 65^\circ$ (CrKβ_1), and $\tan\theta_1^2 - \tan\theta_2^2 \approx 45$, which provided the relative accuracy of determining the lattice parameter of no worse than 10^{-5} [90].

Errors in the Kossel projection method and in other photographic methods are to a great extent due to emulsion shrinkage. This effect can be taken into account by multiplying parameters p, q, and Δx_i, Δy_i in (11) and (14) by the shrinkage coefficient v of the film photoemulsion after the film develops (this coefficient, determined experimentally in [13], was 1.0004).

Another source of the errors may be an increase in the X-ray escape angle $\acute{\alpha}$ in a crystal caused by refraction:

$$\cos\acute{\alpha} = \frac{\cos\alpha}{1 - \delta}, \tag{18}$$

where δ is the refractive index decrement [91, 92] ($\delta \approx 1.3 \times 10^{-6}\rho\lambda^2$, ρ is the sample density [g cm^{-3}], and λ is the wavelength [Å] [12]). Note that, by using the ratios of lengths measured on the photofilm, corrections for the photoemulsion shrinkage and X-ray refraction can be disregarded in most cases.

In measurements of distances on the Kossel projection, errors appear because of the inaccurate determination of its center position and/or the source–detector distance [63]. One more source of errors is the disorientation between a sample and a plane film [93].

The high accuracy of measuring the lattice parameter requires knowledge of the temperature of a crystal under study. Usually, samples in Kossel chambers are thermostated. A special case is Kossel imaging, when an electron beam focused on the sample surface can strongly heat the sample [22, 40].

3. Diffractometric methods for determining interplane distances

Unlike the Kossel projection method, in which the sample and detector positions are stationary and all the reflections are detected simultaneously, diffractometric methods provide the successive detection of X-ray quanta during the movement of a crystal and (or) a detector according to a specified scheme.

3.1 Bond method

The method proposed by Bond in 1960 [94] has a number of advantages (a rather high accuracy ($\Delta d/d \leqslant 10^{-5}$), the simplicity of a device that can be based on a standard diffractometer, a variety of scientific applications) and is widely used for precision measurements of the interplane distances in crystals. If the crystal symmetry is known, the lattice parameter can be calculated from the interplane distance.

The Bond method allows one to determine accurately the Bragg angle for an ideal single crystal using one reflection by measuring directly the angle between the two positions of the crystal (R_1 and R_2 in Fig. 11) for which the Bragg condition

$$2\theta = \pi - |R_2 - R_1| \tag{19}$$

is fulfilled.

The method can be applied for single crystals of any type using a simple or more sophisticated diffractometer [95–103].

The Bond method has been applied for studying the nonstoichiometry in semiconductor GaAs crystals [104–107]; phase transitions in barium-strontium niobate [108–110], vanadium oxide (VO_2) [111], $RbCaF_3$ [112], PbHPO and PbDPO [113], $RbHSeO_4$ [114], and $LiCsSO_4$ [115] crystals; temperature dependences of lattice parameters for silicon [116], germanium [117], GaSb [118], Co [119], diamond [120–122], $KMeF_3$ (*Me* is a metal) [123], sodium nitrite ($NaNO_2$) [124], and V_3O_5 [125] crystals; the influence of deformations on the lattice parameters of GaAs [126–128], DKDP [129], and LiF [130] crystals; the influence of intrinsic point defects on the lattice parameter of Si, Ge crystals and A_3B_5 compounds [131], InSb [132–135], GaAs [136–139], InP [140, 141], InAs [142], GaP [143], and AlAs [144]; the influence of defects appearing upon doping GaAs [145, 146] and GaSb [147] crystals with tellurium, InAs with tin [148], silicon with boron [149–151] and germanium [152], GaAs with silicon [153, 154], YVO_4 with neodymium [155], $GdCa_4O(BO_3)_3$ with Nd^{3+} and Yb^{3+} ions [156], KDP (potassium dihydrophosphate) with Ca, Cr, Fe, and Al metals [157]; and the implantation of nitrogen ions into silicon [158].

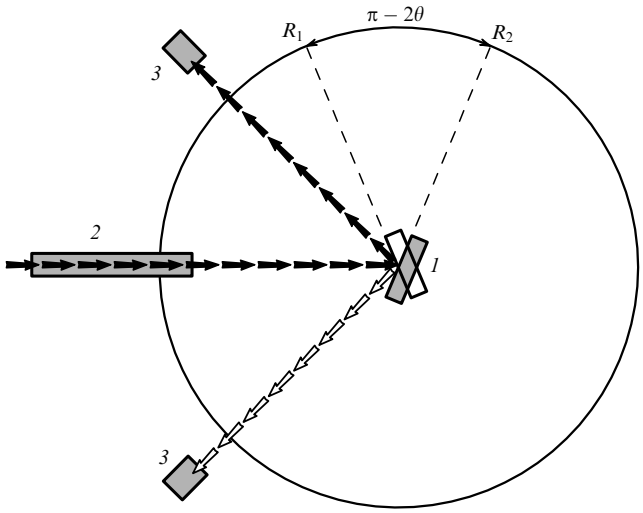

Figure 11. Diagram of a Bond diffractometer: *1* — crystal under study; *2* — collimator; *3* — detectors; R_1 and R_2 are the angular positions of the crystal corresponding to the Bragg reflection [94].

The Bond method works well for studying ideal single crystals with narrow Bragg reflections. Potential eccentricity errors are removed and there is no need to measure the zero angular position of a sample.

The accuracy of the Bond method depends on the accuracy of determining the angular position of the diffraction maximum, which in turn depends on the precision of the mechanics of the single-crystal diffractometer [159]. For example, Baker and coauthors [101] used a specially developed completely automated high-precision APEX diffractometer [160] to measure the crystal lattice parameter with the relative accuracy of 1×10^{-7}.

However, such a high accuracy requires the elimination of systematic errors in measuring lattice parameters [4, 5, 94–96, 161–171]. The main instrumental systematic errors are presented below [4, 5, 172].

(1) The error caused by the deviation of the reflection system of planes from the rotation axis:

$$\frac{\Delta d}{d} \approx \frac{\mu\tau}{\sin\theta} - \frac{\mu^2 + \tau^2}{2}, \tag{20}$$

where μ is the angle between the normal to the reflection plane and a plane perpendicular to the rotation axis of a goniometer and τ is the angle between the beam axis and a horizontal plane. Therefore, $\Delta d/d = 0$ if $\mu = (\tau/\sin\theta)(1 \pm \cos\theta)$. This equation determines optimal adjusting conditions.

(2) The error caused by the vertical divergence $\tau_{\rm div}$ of the primary beam:

$$d_{\rm true} = d_{\rm meas}\left(1 + \frac{1}{6}\left(\frac{\tau_{\rm div}}{2}\right)^2\right). \tag{21}$$

(3) The error caused by the refraction of X-rays:

$$d_{\rm true} = d_{\rm meas}\left(1 + \frac{\delta\cos^2\alpha}{\sin(\theta+\beta)\sin(\theta-\beta)}\right), \tag{22}$$

where α is the angle between the crystal surface and the system of reflection planes, δ is the decrement of the refraction index, and $d_{\rm true}$ and $d_{\rm meas}$ are the true and measured interplane distances.

(4) The error caused by changes in the Lorentz factor and polarization within the reflection curve profile. In this case, the shift of the DRC maximum is described by the expression

$$\Delta\theta = \left(\frac{\Omega}{2}\right)^2 \cot 2\theta\,(2 + \sin^2 2\theta)(2 - \sin^2 2\theta)\,, \qquad (23)$$

where Ω is the DRC full width at the half-maximum.

(5) The temperature error. The error Δd_T in the lattice parameter d caused by the temperature uncertainty ΔT can be estimated from the expression

$$\Delta d_T = d\alpha_d \Delta T \qquad (24)$$

if the thermal expansion coefficient α_d is known in the required crystallographic direction.

(6) The dispersion error. If the wavelength is assigned to the spectral line maximum, this error is absent. However, spectral lines are broad and asymmetric, and this circumstance restricts the accuracy of determining the angular position of the maximum. The diffraction reflection curve can be described by interpolation and approximation by polynomials. However, this approach has serious disadvantages. For example, the result of approximation by a polynomial strongly depends on the polynomial degree [168]. This problem was considered in detail in [170].

Based on the complete convolution model for the diffraction profile, Hartwig and Grosswig [169] analytically obtained all the known errors (and corresponding corrections). Although analytic expressions obtained in [169] are based on some simplifying assumptions, they are usually much more complicated than expressions (20)–(24). The authors showed that, to obtain the relative accuracy of 10^{-7}, all the errors considered by them should be taken into account, although the most important errors are those caused by refraction and the horizontal divergence of an X-ray beam.

It is clear that, to achieve the relative accuracy of $\sim 10^{-7}$, it is also necessary to know with the same accuracy the wavelength used in experiments. For this reason, the authors of [173] presented repeated measurements of the wavelength of the frequently-used CuKα_1 emission line with the accuracy $\Delta\lambda/\lambda \approx 3 \times 10^{-7}$.

In 2000, the authors of [174] proposed a new wavelength standard at the atomic scale instead of the spectral CuKα_1 line wavelength. This is the wavelength λ_M of the ^{57}Fe Mössbauer radiation source, i.e., of the γ radiation line emitted upon a nuclear transition. This line, $\lambda_M = 0.86025474$ Å, was measured with a relative accuracy of 2×10^{-7}. The specific feature of this Mössbauer source is its uniquely small spectral width $\delta\lambda/\lambda = 3.5 \times 10^{-13}$ and also the excellent reproducibility (with an accuracy of $\sim 10^{-11}$) independently of external factors such as temperature and pressure.

In many cases, determining one interplane distance is insufficient to characterize the real structure of a crystal. In the Bond method, uncertainties in the value of corrections for compensating some systematic and instrumental errors are excluded, as a rule, using symmetric reflections [165]. One sample of the matter under study is sufficient for determining the lattice parameter in the case of cubic crystals, but two samples are necessary for tetragonal and hexagonal systems, and three samples are necessary for the orthorhombic system. The difficulty increases in the study of nonorthogonal lattices. To eliminate these difficulties, the Bond method was supplemented in [5] with measurements of several asymmetric crystal planes 'working' both in reflection and transmission with small Bragg angles. Measurements are performed for lattice planes with diffraction vectors parallel to the vectors of the unit cell. The disadvantages of this modified method are the strict requirements for preparing a sample, the restricted choice of reflections, and the low measurement accuracy due to the use of reflections with small Bragg angles.

The principle of determining lattice parameters based on the measurement of angles between the four positions of a crystal for which the Bragg condition is fulfilled is described in [168]. This method can be used to characterize more efficiently the real structure of single crystals due to measurements of the three coplanar geometrical lattice parameters with a high accuracy in the same region of a sample in one measurement cycle.

Despite the difficulties mentioned above, the Bond method was used to study a number of low-symmetry crystals [102, 109, 111, 115, 124, 125, 156, 175, 176]. For example, the lattice parameters of lithium-cesium sulfate $LiCsSO_4$ were measured [115] in the temperature range of 160–550 K using an X-ray single-crystal Bond diffractometer. The Bragg angles of reflections (12 0 0), (0 6 0), (6 6 0), and (0 0 10) were measured using CuKα_1 radiation. The relative accuracy of measuring lattice parameters was no worse than 10^{-5}.

The lattice parameters of $PbHPO_4$ single crystals were measured [113] in the vicinity of the ferroelectric phase transition at $T = 310$ K. The deuterated $PbDPO_4$ crystal was measured only in the ferroelectric phase because of changes in the real structure at higher temperatures. To obtain the high accuracy, the diffraction reflections (800), (080), and (406) were chosen for CuKα_1 and (008) for CuKβ with Bragg angles at 84°, 68°, 78°, and 76°, respectively. The position of the reflection curve maximum was determined with an accuracy of about 4″. This gave the dimensions of the unit cell with the relative error of 2×10^{-6} for the parameter a, 5×10^{-6} for b, and 8×10^{-6} for c.

The lattice parameters of strontium–barium niobate $Sr_xBa_{1-x}Nb_2O_6$ (SBN) in [109] were measured using reflections (16 0 0) ($\theta = 80.879°$) and (16 1 0) ($\theta = 82.451°$) to determine the parameter a and the reflection (005) ($\theta = 78.146°$) for the parameter c. The relative errors at room temperature were estimated as $\delta a/a = 6 \times 10^{-6}$ and $\delta c/c = 3 \times 10^{-6}$.

Returning to the problem related to the natural width and asymmetry of an X-ray spectral line, note that it can be solved using a crystal monochromator placed in front of a sample, as in paper [97] (Fig. 12). In this case, the experimental width of the DRC can be optimized by decreasing the width of the instrumental function. The instrumental function of a single-crystal diffractometer depends on the angular and spectral divergence of an X-ray beam incident on a crystal sample, while this function for a two-crystal diffractometer depends on the angular divergence of a beam formed with a monochromator and on the beam dispersion D:

$$D = \frac{\Delta\lambda}{\lambda}|\tan\theta_M \pm \tan\theta_0| = \frac{\delta\lambda}{\lambda}\frac{\sin(\eta/2)}{\cos\theta_0\cos\theta_M}\,. \qquad (25)$$

Here, $\Delta\lambda/\lambda$ is the relative width of the spectral line, θ_M and θ_0 are the Bragg angles of the monochromator and sample, respectively, η is the angle between the directions of the primary beam and the beam at the sample output

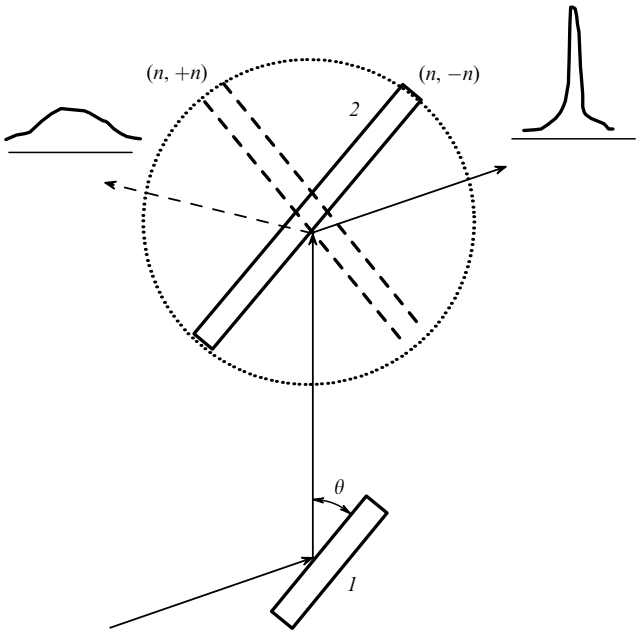

Figure 12. Diagram of a two-crystal Godwod diffractometer [97]: *1* — crystal monochromator; *2* — crystal under study (position corresponding to the antiparallel $(n, +n)$ diffraction geometry is shown by the dashed line) (see text).

$(\eta = 2|\theta_M \pm \theta_0|)$, and the signs '−' and '+' correspond to the nonparallel and antiparallel diffraction schemes, for which the notation $(n, -m)$, $(n, +m)$ is accepted, respectively, emphasizing differences in the interplane distances of the reflection planes of two crystals (when they are equal for $\eta = 0$, we are dealing with the parallel diffraction geometry $(n, -n)$).

The dynamic theory of X-ray scattering [91, 177] gives the width of the X-ray DRC for an ideal crystal in the form

$$\Omega = \frac{2C|\chi_{hr}|}{b^{1/2}\sin 2\theta}\,, \tag{26}$$

where χ_{hr} is the real part of the Fourier component of the crystal polarizability; the polarization factor $C = 1$ for the wave field component polarized perpendicular to the scattering plane (σ polarization) and $C = \cos 2\theta$ for the component polarized in this plane (π polarization); and $b = \gamma_i/\gamma_e$ is the asymmetry coefficient for Bragg reflection, where γ_i and γ_e are the direction cosines of the incident and diffracted X-rays, respectively, $\gamma_i = \sin(\theta - \alpha)$, $\gamma_e = \sin(\theta + \alpha)$, and α is the angle between reflection surfaces and the crystal surface, which can be both positive and negative.

It follows from (26) that the angular divergence of the beam formed with a monochromator can be made quite small by decreasing χ_{hr} using a monochromator consisting of light elements and/or reflections with large Miller indices, and also by using asymmetric diffraction.

It is clear that, to eliminate the beam dispersion D (expression (25)), it is sufficient to direct the angle η to zero, i.e., to select the reflections of the monochromator and the crystal under study so that the corresponding interplane distances (and, therefore, Bragg angles) are close. This condition greatly restricts the applications of the method because crystalline materials have, generally, different (although sometimes close) interplane distances, so that a certain monochromator is required for each experiment [178]. Nevertheless, a two-crystal diffractometer cannot always be used in the Bond method, because one of the diffraction geometries is the nonparallel $(n, +n)$ scheme, which leads to the formation of a broad diffraction line (see Fig. 12).

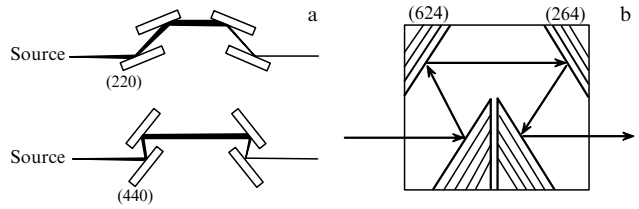

Figure 13. Trajectory of beams (a) in a four-crystal $(+n, -n, -n, +n)$ Bartels monochromator upon diffraction from reflecting (220) and (440) planes [177] and (b) in a monoblock silicon monochromator for $(+n, -n, -n, +n)$ with SR using {642} reflections and forming a beam with $\lambda = 1.343819$ Å [180].

Another way to eliminate the influence of the beam dispersion D on the DRC width is the drastic narrowing of the transmission band of the monochromator. In practice, for this purpose, as a rule, a three-crystal diffractometer with a two-crystal monochromator in the antiparallel $(n, +m)$ diffraction scheme is used. In this case, the spectral bandwidth $(\Delta\lambda/\lambda)_{nm}$ and the angular divergence Ω_{nm} of such a monochromator are described by the expressions [179]

$$\left(\frac{\Delta\lambda}{\lambda}\right)_{nm} = \frac{\Omega_n b_n^{1/2} + \Omega_m b_m^{-1/2}}{\tan\theta_n + \tan\theta_m}\,, \tag{27}$$

$$\Omega_{nm} = \frac{(\Omega_n b_n^{1/2} + \Omega_m b_m^{-1/2})\tan\theta_m}{\tan\theta_n + \tan\theta_m} - \Omega_m b_m^{1/2}\,, \tag{28}$$

where indices n and m correspond to the first and second crystals of the monochromator.

A four-crystal monochromator consisting of two monolithic monochromators with grooved channels (channel-cut monochromators) was created by Bartels [100]. Two additional reflections are used to compensate the deviation of the beam from its initial direction (Fig. 13a). Ge(440) reflections were used. The angular divergence of the obtained beam was 5″, and a narrow region with $(\Delta\lambda/\lambda)_{nm} = 2.3 \times 10^{-5}$ was cut from the broad CuKα$_1$ spectral line ($(\Delta\lambda/\lambda)_{sp} = 2.88 \times 10^{-4}$ [181]). Thus, the geometry and properties of a four-crystal monochromator are ideal for the construction of a high-resolution multifunctional X-ray diffractometer. This conclusion is also confirmed in paper [102], where an X-ray beam with $(\Delta\lambda/\lambda)_{nm} = 1.28 \times 10^{-4}$ and $\Omega_{nm} = 11''$ was formed using a germanium Bartels monochromator (*3*) with four successive Cu(220) reflections (Fig. 14). To increase the reliability of measurements, the directions $2\theta^+$ and $2\theta^-$ of diffracted beams with respect to the primary beam were measured by germanium monolithic crystal analyzers with cut channels (*5*) with an accuracy of 11″ simultaneously with the corresponding positions ω^+ and ω^- of the samples (see Fig. 14).

However, the spectral narrowing of the X-ray beam considerably reduces its intensity. Therefore, it is necessary to use a brighter SR source, as was done for the first time in [182]. The authors of [182] used a monoblock monochromator (Fig. 15) with successive reflections $(\bar{5}\,3\,\bar{5})-(3\,3\,5)$ or $(1\,3\,\bar{1})-(3\,1\,\bar{1})$, which produced a strongly collimated beam with a very narrow transmission band. The calculated angular divergence and transmission band for reflections $(\bar{5}\,3\,\bar{5})-(3\,3\,5)$ are 3.2×10^{-6} rad and 1.7×10^{-6}, respectively, and 4.5×10^{-5} rad and 1.5×10^{-5} for reflections

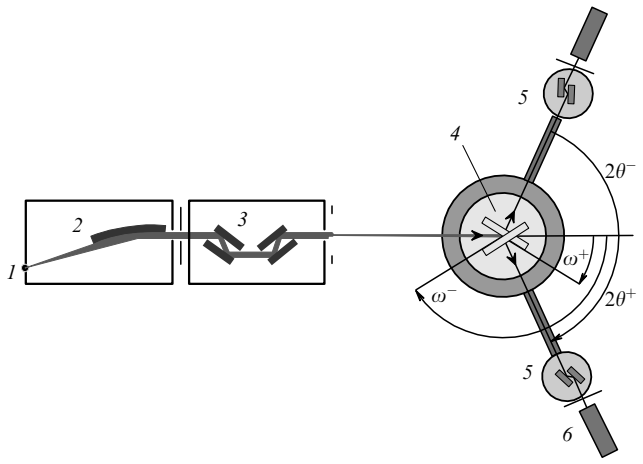

Figure 14. Diagram of the experimental setup used in [102]: *1* — radiation source (X-ray tube with a copper anode), *2* — parabolic multilayer mirror, *3* — Bartels monochromator, *4* — crystal under study, *5* — Ge(220) analyzers mounted in front of detectors (*6*). The two positions of the sample (ω^+ and ω^-) and detector ($2\theta^+$ and $2\theta^-$) supplementing each other illustrate the extended Bond technique.

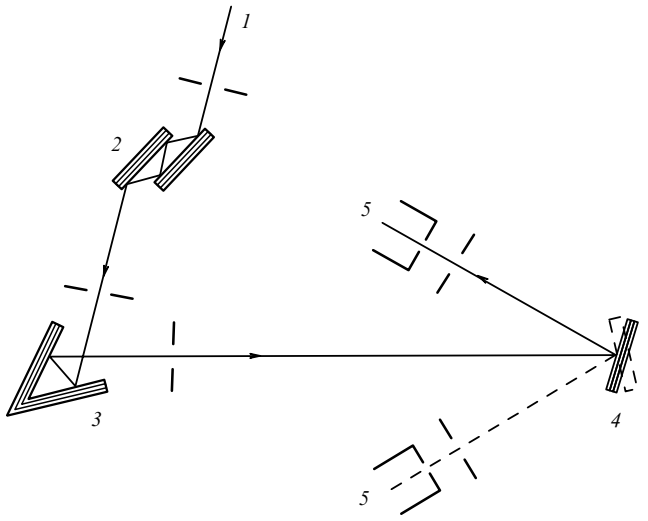

Figure 15. Diagram of the setup for precision measurements of the lattice parameter by the Bond method using SR: *1* — SXR beam, *2* — preliminary monochromator, *3* — monoblock silicon monochromator, *4* — crystal under study, *5* — detectors [106].

$(1\,3\,\bar{1})-(3\,1\,\bar{1})$. The output wavelength of the monoblock monochromator is determined by the interplane distances of reflection planes and the angle between these planes. Monochromators were calibrated using a high-quality silicon-crystal standard. The wavelengths for the $(\bar{5}\,3\,\bar{5})-(3\,3\,5)$ and $(1\,3\,\bar{1})-(3\,1\,\bar{1})$ reflections were 1.3536 and 1.3965 Å, respectively.

In [106, 183], the GaAs lattice parameter (reflection (008)) was determined with a relative accuracy of 5.9×10^{-6} using a monolithic monochromator with reflections $(\bar{5}\,3\,\bar{5})-(3\,3\,5)$.

The authors of [184] proposed several types of monoblock monochromators for SR which can provide the fixed position of the output beam without changing the direction of the primary beam (Fig. 13b), which is convenient for adjusting X-ray optics. The high-precision measurements of the lattice parameter were performed for GaAs samples using a system based on a monolithic silicon $(+n, -n, -m, +m)$ monochromator (Fig. 13b). The output monochromatic beam with the wavelength $\lambda = 1.396563$ Å is parallel to the incident beam after four successive reflections of $(2\,\bar{4}\,\bar{2})$, $(\bar{2}\,4\,2)$, $(5\,1\,1)$, and $(\bar{5}\,\bar{1}\,\bar{1})$. The precision of measuring the lattice parameter for the (008) reflection ($\theta = 81.14^\circ$) was estimated as 4×10^{-8}. In [185], the silicon lattice parameter (reflection (444)) was determined with a relative accuracy of 6.2×10^{-7} with the help of a monolithic silicon $(+n, +m, -m, -n)$ monochromator with reflections of $(1\,1\,7)$, $(1\,5\,1)$, $(\bar{1}\,\bar{1}\,\bar{7})$, and $(\bar{1}\,\bar{5}\,\bar{1})$ and $\lambda = 1.410846$ Å.

3.2 Four-crystal spectrometer method

Another method for measuring lattice parameters was proposed in [186]. Diffraction angles were measured with a special diffractometer in which a crystal and a detector are fixed in the reflection position. The angle between the incident and reflected beams was measured with the help of Soller slits [187], which restrict the divergence of the incident and diffracted beams and at the same time eliminate errors related to the eccentricity and X-ray absorption. This procedure does not involve restrictions concerning the size and shape of the irradiated region or the crystal perfection, thereby eliminating systematic errors due to these reasons [188, 189]. Measurements for silicon with a standard relative error of 3×10^{-6} ($\theta \approx 79^\circ$) were performed in [186].

A high-resolution four-crystal diffractometer, proposed in [190], provides very accurate measurements of diffraction angles. The Bartels monochromator (*2*) (Fig. 16) provides a very narrow spectral transmission band. A crystal analyzer (*4*) will reflect only X-rays lying in the angular region of its own DRC. Therefore, here, it is the diffracted beam direction that is important, rather than the sample position. Thus, the problem of sample eccentricity is absent. To measure accurately the scattering angle, the zero angle ($2\theta = 0$) can be determined very accurately with a crystal analyzer. This method can be applied to many materials (high-quality single crystals and polycrystalline samples), because it requires only one measurement. The uncertainty of the analysis of different volumes (possible during a change in the sample position for the second measurement of the diffraction angle) is eliminated, while the primary beam has a small spectral divergence. Here, the accuracy of measuring the lattice parameter is comparable to the accuracy of the Bond method; however, the diffractometer requires a high-quality precision goniometer and careful adjustment [3, 191–193].

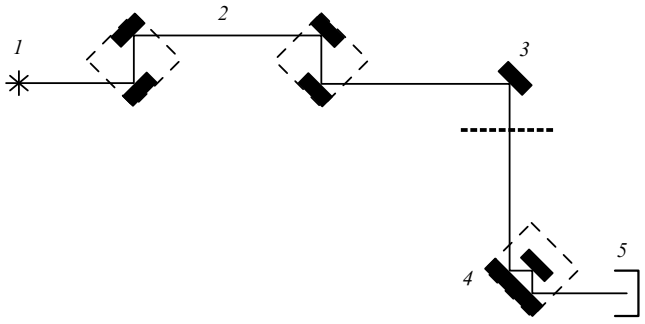

Figure 16. Diagram of a four-crystal diffractometer [190]: *1* — X-ray source, *2* — Bartels monochromator, *3* — sample, *4* — analyzer, *5* — detector.

3.3 Backscattering method

Backscattering (BS) was first considered in the dynamic theory of X-ray diffraction in an ideal crystal in 1972 [194]. Two interesting BS features were pointed out already in this early study: as the Bragg angle approaches 90°, the spectral transmission band of the crystal drastically decreases, whereas the width of its DRC drastically increases ($\Omega = (2|\chi_{hr}|)^{1/2}$). Thus, it is possible to create high-energy resolution wide-aperture optical devices based on BS. Later, many publications appeared devoted to the application of X-ray BS in high-resolution X-ray optical devices and metrology and also for structural studies of various crystal objects [195–197].

As follows from the Wolf–Bragg equation, the X-ray diffraction sensitivity to a change in the interplane distance is proportional to $\tan\theta$. The first papers devoted to precision measurements of lattice parameters using Bragg angles close to 90° appeared already in the 1970s [198–201]. In these papers, two-crystal diffractometers were used with crystals arranged in the parallel $(n, -n)$ or quasi-parallel $(n, -m)$ geometry, eliminating in this way dispersion, which is especially noticeable at large Bragg angles. Later, a high-angle two-crystal X-ray diffractometer (HADOX) was created [202–205], providing a relative accuracy of 10^{-6}. The method proved to be useful for studying structural phase transitions in $KMnF_3$ [206] and $SrTiO_3$ [207, 208] crystals, for investigations of the block structure in $BaTiO_3$ crystals [209–211], and for studying the deformation in silicon crystals at low temperatures [212]. The authors of [204] believe that, if for $\theta = 79°$ the relative accuracy of measuring the silicon lattice parameter can be about 10^{-7}, then for $\theta = 89.99°$, the expected accuracy can be $\sim 10^{-10}$.

Wavelength λ_c corresponding to the center of the BS spectral region is determined by the expression

$$\lambda_c \approx 2d\left(1 - \frac{\Delta^2}{2} - w\right). \qquad (29)$$

Equation (29) is the general condition of Bragg backscattering, which includes not only a deviation from the exact normal reflection angle $\Delta = \pi/2 - \theta \ll 1$, but also the refraction correction w. Due to the Δ^2 dependence in (29), the deviation from the exact normal reflection condition even by a small angle, for example, $\Delta \approx 0.1$ mrad, changes the reflected wavelength only by $5 \times 10^{-9}\lambda_c$. Therefore, for $\Delta \leqslant (2|\chi_{hr}|)^{1/2}$, the lattice parameter is weakly sensitive to the Bragg angle. It seems that, for this reason, the accuracy of measuring the lattice parameter achieved in papers [122, 213] using the Bond method was no better than 10^{-6}. If $\Delta \leqslant (2\varepsilon)^{1/2}$, where ε is the required relative measurement error, then a simple relation $\lambda_c = d(1 - w)$ is valid even for relatively rough angular adjustments. For example, $\Delta \leqslant 100$ μrad provides the relative uncertainty $\varepsilon \approx 10^{-8}$. This property is used to 'transfer' the interplane distance d to the instrument scale, which chooses and measures X-ray wavelengths [195, 196, 214]. It is clear that the accuracy of measuring crystal lattice parameters directly depends on the accuracy of measuring the wavelength of the beam incident on a sample.

The authors of papers [214, 215] used γ radiation from ^{57}Fe as the wavelength ethalon. Recall that the wavelength of γ radiation from ^{57}Fe ($\lambda_M = 0.86025474$ Å) was measured with a relative accuracy of 2×10^{-7} [174]. The working wavelength was changed with a silicon monoblock channel-cut monochromator used as a λ meter. The symmetric (777) reflection was used. If the output radiation wavelength of the λ meter (*2*) (Fig. 17) coincides with λ_M, the ^{57}Fe nuclei in an α-Fe foil (*3*) behind the λ meter are coherently excited. The excited nuclei directly emit coherent Mössbauer photons [216, 217]. Detector (*4*) (a semi-transparent silicon avalanche photodiode) [218] with a time resolution of 0.7 ns was mounted directly behind the λ meter at a distance of 6 m from the crystal. The transmitted radiation was reflected from an α-Al_2O_3 crystal and was incident on the detector with a 40-ns delay, allowing one to distinguish easily the reflected pulse from the incident one. The sapphire lattice parameters were determined by measuring the rotation angle ψ_{hkil} of the λ meter at which it 'selects' X-rays corresponding to the backscattering of the sapphire (*hkil*) reflection and the reference angle ψ_M at which the sample reflects Mössbauer radiation. The α-Al_2O_3 lattice parameters were measured in the temperature range from 4.5 to 374 K with relative errors below 6×10^{-6}. This accuracy is more than an order of magnitude lower than the expected accuracy of 10^{-7}, which is the theoretical limit of the experimental equipment used. The main sources of errors were the large angular beam divergence at the λ meter output and defects in the α-Al_2O_3 crystal, as well as temperature oscillation inside the experimental station during measurements [214, 215].

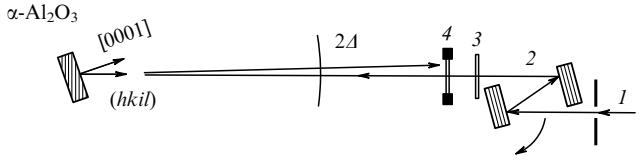

Figure 17. Experimental setup for measuring sapphire lattice parameters: *1* — SR beam, *2* — λ meter (Si channel-cut crystal), *3* — α-Fe foil, *4* — detector (semiconductor silicon avalanche photodiode) [214, 215].

A variable parameter in papers [219–222] is the X-ray energy measured with a high-resolution many-crystal monochromator calibrated by a perfect silicon crystal reference with the lattice parameter $a = 5.43101901$ Å [223].

For example, a monochromator in [220] consisted of two monolithic silicon channel-cut blocks embedded into each other [224] ($\Delta E = 1.0$ meV, which corresponds to $\Delta a/a = 4.6 \times 10^{-8}$) (Fig. 18). Energy was tuned by rotating the inner block with respect to the external one.

The Bragg angle was 89.986°. The X-ray energy was 21.56 eV and (5 1 19) and (7 7 17) reflections corresponding to the same Bragg angle were used. The error of measuring the germanium lattice parameter did not exceed $\pm 2 \times 10^{-6}$ Å, which corresponds to $\delta a/a \approx \pm 3.5 \times 10^{-7}$.

Using a high-resolution monochromator with the transmission band $\Delta\lambda/\lambda \approx 4 \times 10^{-8}$ consisting of six silicon

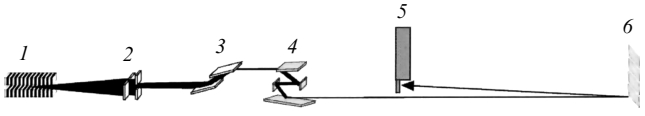

Figure 18. Experimental setup for measuring the Ge lattice parameter: *1* — built-in element of the storage ring of a synchrotron, *2* — system of slits, *3* — preliminary SR monochromator, *4* — high-resolution monochromator, *5* — detector, *6* — set of Ge crystals under study [220].

crystals [225], the authors of papers [221, 222] determined parameters of the diamond lattice with a uniquely high relative accuracy of 1.2×10^{-8}.

4. Diffractometric methods for determining lattice parameters

4.1 Method of two coplanar reflections

The authors of paper [226] proposed to determine the lattice parameter of cubic syngony crystals from the angle Ψ_0 (Fig. 19) between diffraction maxima corresponding to two coplanar reflections (i.e., reflections for which diffraction planes coincide) under the condition that the difference between the angles of incidence of the X-ray beam on a crystal under study for them be small enough ($\Psi_0 < 1^\circ$). It is clear that the rotation of a sample through such a small angle should not deteriorate the method locality.

The relation

$$\Psi_0 = \varphi_{1,2} - |\theta_1 - \theta_2| \tag{30}$$

is valid, where θ_1 and θ_2 are Bragg angles corresponding to the $(h_1k_1l_1)$ and $(h_2k_2l_2)$ reflection planes, and $\varphi_{1,2}$ is the angle between these planes.

To determine the lattice parameter of a cubic syngony crystal, it is sufficient to measure the angle Ψ_0. The method accuracy is determined by the expression

$$\frac{\delta a}{a} = \varepsilon(\delta\Psi_0)\,, \tag{31}$$

where $\delta\Psi_0$ is the accuracy of measuring the angular distance between diffraction maxima, and the parameter $\varepsilon = |\tan\theta_1 - \tan\theta_2|^{-1}$ characterizes the precision of the method.

The method requires the introduction of correction for refraction [226]. The accuracy of measuring the absolute value of the lattice parameter depends on the accuracy of adjusting a sample. The adjustment becomes simpler if the diffraction vector of one of the reflections virtually coincides with the azimuthal axis of the diffractometer lying in the diffraction plane. Then, the rotation of the sample around this axis — required to adjust the second reflection — will not lead to the readjustment of the first reflection. Therefore, the method of successive approximations can usually provide a rather accurate crystal alignment [227]. The measurement of the relative change in the crystal lattice parameter (for example, over the area or along the sample) does not impose strict requirements on the crystal adjustment accuracy. Thus, the homogeneity of a crystalline GaAs plate with the (111) surface orientation was studied in [178] using a two-crystal X-ray diffractometer, CuKα_1 radiation, a pair of Bragg asymmetric reflections (331)–(440), and the symmetric (333) reflection of a germanium monochromator. Here, the angle $\varphi_{1,2}$ between the (331) and (440) planes is 13.26°, and the corresponding Bragg angles are 36.44° and 50.42°, $\Psi_0 = -0.72^\circ$, and $\varepsilon = 2.12$. Because the distance between corresponding diffraction maxima in this experiment was determined with an accuracy of at least $0.8''$, the error of measuring the relative change in the lattice parameter did not exceed 8×10^{-6}.

This method can be used to characterize a broad class of cubic syngony crystals, because, for any X-rays, it is always possible to find one or even several pairs of coplanar reflections with a small enough angular distance between corresponding diffraction maxima sensitive to small changes in the crystal lattice parameter. Note that the probability of finding such pairs increases upon increasing the ratio a/λ.

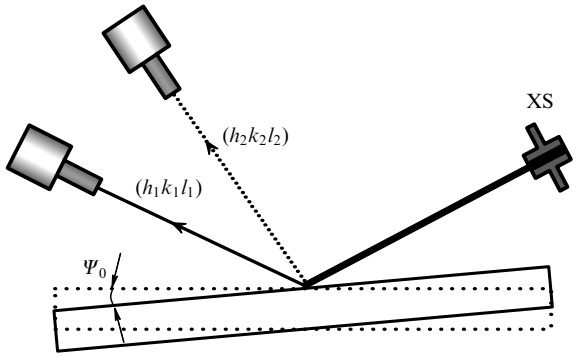

Figure 19. Diagram of coplanar diffraction for two $(h_1k_1l_1)$ and $(h_2k_2l_2)$ reflections. Ψ_0 is the angular distance between diffraction maxima, XS is a slit forming the size of a monochromatic X-ray beam.

It follows from (30) that, to increase the sensitivity of the method, a substantial difference between Bragg angles θ_1 and θ_2 is desired. But one should bear in mind that the chromatic dispersion between the first crystal (monochromator) and the sample should be taken into account. The dispersion depends on the difference between Bragg angles θ_1 and θ_2. Thus, to reduce the dispersion, the difference between θ_1 and θ_2 should be small. This conclusion contradicts the first condition. For this reason, the choice of two optimal reflection surfaces is not always simple [226].

The method of determining crystal lattice parameters with the help of two coplanar reflections was developed in [228, 229] for middle syngony crystals. KDP is a crystal of the tetragonal syngony with lattice parameters $a = b = 7.453$ Å and $c = 6.959$ Å, but, with the help of the $\{hk0\}$ reflections ((420) and (280) in the given case), it is possible to determine precisely the relative values of parameters $a = b$. The degree of homogeneity of a (110) KDP sample was studied in [228] using CoKα_1 radiation and the (420) and (280) reflections. Unlike the geometry of experiments shown in Fig. 19, where both diffracted beams are on one side of the primary beam, here, diffracted beams are located on different sides of the beam. In this case, $\varepsilon = (\tan\theta_1 + \tan\theta_2)^{-1}$, and expression (30) takes the form

$$\Psi_0 = (180^\circ - \varphi_{1,2}) - (\theta_1 + \theta_2)\,. \tag{32}$$

The X-ray beam incident on the sample was formed with a Ge (111) crystal monochromator using strongly asymmetric (311) reflection. Such a monochromator provides a small enough divergence of incident radiation in the horizontal plane ($\sim 1.7''$), making possible an almost nondispersion setup for the (420) reflection. The distance between diffraction maxima was determined with a high accuracy ($\delta\Psi_0 \approx 0.6''$), which was facilitated by the location of the narrow DRC of the (420) reflection on the slope of the broad DRC of the (280) reflection. Bragg angles for the (420) and (280) reflections are equal to 32.46° and 81.76°, respectively. Therefore, $\varepsilon = 0.1326$, and the relative accuracy of measuring the KDP crystal lattice parameter, according to (30), was no worse than 6×10^{-7}.

The authors of [229] studied the local variations of lattice parameters in a tetragonal paratellurite TeO_2 crystal and

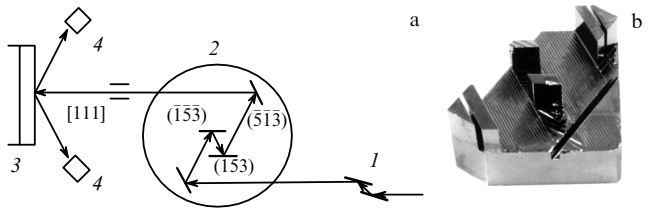

Figure 20. (a) Schematic of a diffractometer for relative measurements of interplane distances using SR: *1* — preliminary SR monochromator, *2* — monolithic silicon monochromator, *3* — sample, *4* — detectors; (b) monolithic monochromator *2* for the wavelength 1.612607 Å [185] (see text).

a trigonal lanthanum–gallium tantalite $La_3Ga_{5.5}Ta_{0.5}O_{14}$. Using a pair of reflections found, the variation in the lattice parameter a along the surface of these crystals was determined with the help of a laboratory X-ray source. The relative measurement accuracy was 4×10^{-6}, for a spatial resolution of 140 μm.

A high-resolution diffractometer for relative measurements of interplay distances using SR was described in [185]. A monolithic silicon monochromator using the (5 1 3), (1 5 3), ($\bar{5}$ $\bar{1}$ $\bar{3}$), and ($\bar{1}$ $\bar{5}$ $\bar{3}$) reflections in the dispersion $(+n, +n, -n, -n)$ scheme forms a $\lambda = 1.612607$ Å X-ray beam with angular and spectral divergences of 0.1×10^{-6} rad and 4.3×10^{-6}, respectively. The beam wavelength satisfies the condition of the quasi-simultaneous Bragg diffraction for the (5 1 3) and (1 5 3) reflections of the (111) silicon crystal (Fig. 20) under study. The Bragg angle is determined by the expression [180]

$$\theta = 90^\circ - \frac{\varphi_{1,2}}{2} - \frac{\Psi_0}{2}\,, \tag{33}$$

where $\varphi_{1,2}$ is the angle between the (5 1 3) and (1 5 3) reflection planes. Note that expression (33) is equivalent to (32) for $\theta_1 = \theta_2 = \theta$.

The use of a monoblock silicon monochromator for SR with reflection pairs (624) and (264) in the antiparallel diffraction scheme $(+n, -n, -n, +n)$ with $\lambda = 1.343819$ Å (Fig. 13b) provided a relative measurement accuracy on the silicon crystal of $\sim 10^{-8}$ [180]. Using large Bragg angles ($\theta = 82.03^\circ$) in a silicon SR monochromator with reflection pairs (10 0 2) and (10 2 0) ($\lambda = 1.055$ Å), the authors of [230–234] improved the method accuracy to $\delta a/a = 3 \times 10^{-9}$.

4.2 Renninger method

Multiwave (multiray) diffraction, unlike simple Bragg (so-called two-ray) reflection, occurs when not one, but several systems of atomic planes in a crystal are simultaneously in the position corresponding to the diffraction reflection of an incident X-ray beam. In the reciprocal space language, the effect appears when two or more points of the reciprocal lattice simultaneously lie on the Ewald sphere surface [235–237]. The geometry of experiments performed for the first time by Renninger [238] is shown schematically in Fig. 21. A crystal is placed in a position corresponding to the Bragg two-ray reflection, for example, symmetric S_1 from the $(h_1k_1l_1)$ planes. A detector with a widely open window remains at rest and aligned to the S_1 reflection. Then, the crystal is rotated around the reflection diffraction vector S_1, not violating the alignment to this reflection. For some azimuthal position of the crystal with respect to the incident beam, in addition to reflection from the $(h_1k_1l_1)$ planes, reflection from another

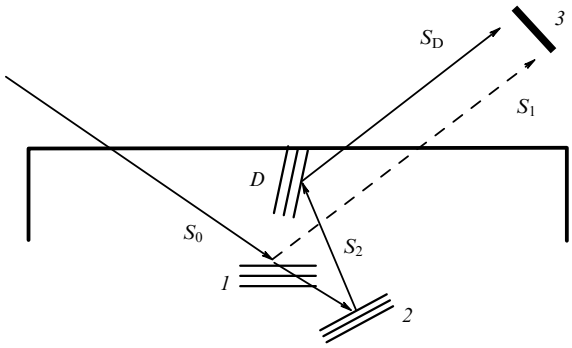

Figure 21. Scheme of double reflection in a single crystal: *1*, *2*, and *D* are the $(h_1k_1l_1)$, $(h_2k_2l_2)$, and $(h_Dk_Dl_D)$ reflection planes, respectively; S_0, S_1, S_2, and S_D are the primary beam and beams reflected from the $(h_1k_1l_1)$, $(h_2k_2l_2)$, and $(h_Dk_Dl_D)$ planes; *3* is a detector (reflection S_1 corresponds to the forbidden $(h_1k_1l_1)$ reflection and is denoted by the dashed line).

family of planes $(h_2k_2l_2)$ is also possible. It can be shown that some third family of planes $(h_Dk_Dl_D)$ in the crystal finds itself in the reflection position for the reflected beam S_2, i.e., the Bragg condition is fulfilled for $(h_Dk_Dl_D)$ planes (see Fig. 21). In other words, in this case, double reflection is observed: the beam first reflected from the $(h_2k_2l_2)$ planes in the direction S_2 is then reflected from the $(h_Dk_Dl_D)$ planes in the direction S_D. Thus, the doubly reflected beam S_D propagates in the same direction as the beam S_1 that experienced the usual single reflection, the reflection indices being related by the equalities

$$h_1 = h_2 + h_D\,, \quad k_1 = k_2 + k_D\,, \quad l_1 = l_2 + l_D\,. \tag{34}$$

Renninger called this phenomenon 'indirect excitation' (Umweganregung).

Usually, the first reflection with a very low intensity or forbidden by the spatial group of the crystal is chosen. Its intensity determines the background diffraction intensity, which should be low. Due to the azimuthal rotation, diffraction conditions are satisfied successively for other planes, and a typical diffraction pattern consists of a system of multiwave maxima (reflections) (Fig. 22). It contains information obtained from different crystallographic directions from which the unit cell parameters can be determined with good accuracy. Multiwave diffraction involves three or more beams diffracted and redirected by the different sets of planes inside the crystal (compared to two beams for 'normal' diffraction); conditions for multiwave diffraction are more critical than those for Bragg diffraction, while the diffraction peaks are correspondingly narrower and therefore can be measured more accurately.

The azimuthal position φ of a multiwave diffraction peak depends on the radiation wavelength and crystal lattice parameters. There are two azimuthal positions usually called 'input–output' and 'output–input,' in which the same secondary reflection S_2 is excited: $\varphi_1 = \alpha - \beta$ and $\varphi_2 = \alpha + \beta$ (α is the angle between the vector $\mathbf{p}$ and the diffraction plane of the first reflection). The procedure of accurate measurements of lattice parameters involves measurements in both positions.

For simplicity, vectors $\mathbf{g}$ and $\mathbf{p}$ are used as reciprocal lattice vectors for the first and second reflections. Vectors $\mathbf{p}_n$ and $\mathbf{p}_p$ are the components of the vector $\mathbf{p}$ perpendicular and parallel to the vector $\mathbf{g}$. For a given wavelength, the moduli of vectors $\mathbf{g}$, $\mathbf{p}$, $\mathbf{p}_n$, and $\mathbf{p}_p$ are the functions of lattice parameters

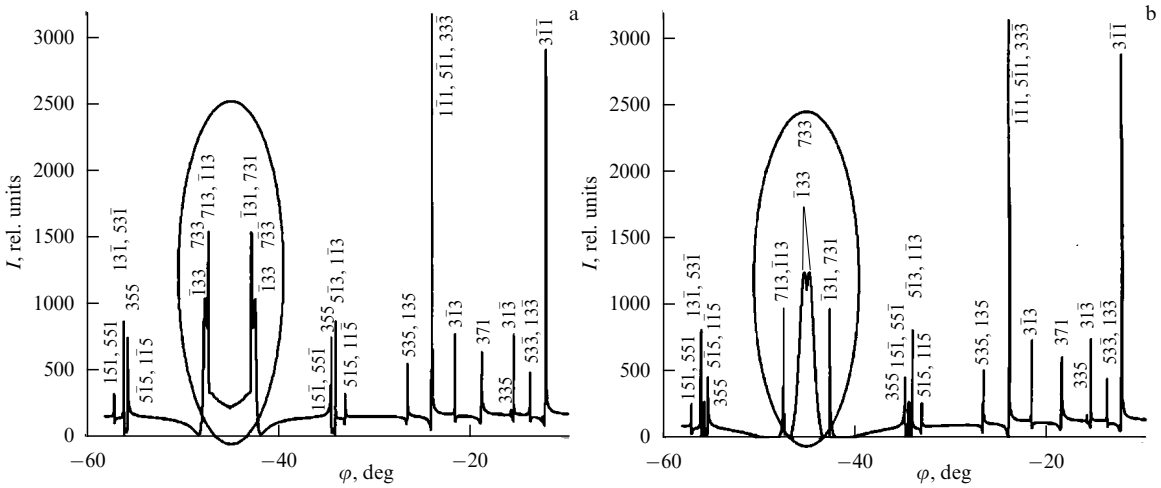

Figure 22. Diffractograms calculated for (a) a $Cd_{0.96}Hg_{0.04}Te$ ($a = 6.4814$ Å) crystal and (b) a $Cd_{0.79}Hg_{0.21}Te$ ($a = 6.47802$ Å) crystal at $T = 20\,^{\circ}C$. $CuK\alpha_1$ radiation was used [245] (see text).

and Miller indices. For determining lattice parameters and indexing diffractograms, the expression [236, 239, 240]

$$\cos\beta = \frac{(p^2 - p_{\rm p}g)^{1/2}}{2p_{\rm n}\left[(1/\lambda)^2 - (g^2/4)\right]^{1/2}} \tag{35}$$

can be used.

However, before determining the lattice parameters, it is necessary to index the repeated diffraction pattern. The principle of the indexation method is known as the reference vector method [236, 239, 240]. The UMWEG computer program [241, 242] can be very useful for rather complicated calculations and for the graphical presentation of the multiwave diffraction. Another analytic indexation method was described in [243].

Expression (35) is valid for all the crystal syngonies. In practice, however, it is mainly used for cubic crystals, and a special approach is required to adapt the method to other (rectangular) systems [244]. For cubic syngony crystals,

$$a = \frac{\lambda(p^2 - p_{\rm p}g)}{2p_{\rm n}\cos\theta_{\rm G}\cos\beta}\,, \tag{36}$$

where the angle $\theta_{\rm G}$ is the Bragg angle for the first reflection and a is the lattice parameter.

The differentiation of (36) gives the expression

$$\frac{\delta a}{a} = \tan\theta_{\rm G}\,\Delta\theta_{\rm G} + \tan\beta\,\Delta\beta\,. \tag{37}$$

Because the angle $\theta_{\rm G}$ is the same for all multiple diffractions upon the first reflection, the ratio $\delta a/a$ depends on the second reflection via the angle β. Therefore, multiple diffraction with small β is preferable for the accurate measurement of a.

Figure 22 presents parts of diffractograms for the $Cd_{1-x}Hg_xTe$ compound with different compositions (x) [245]. Diffractograms were qualitatively and quantitatively analyzed using the UMWSEG-98 program [241]. One can see that the position of a pair of 'mirror' (input–output and output–input) peaks $(\bar{1}33)/(733)$ and $(133)/(7\bar{3}\bar{3})$ (shown in ovals) is sensitive to a change in the lattice parameter.

The Renninger multiwave diffraction method provides the measurement of the crystal lattice parameters with the relative accuracy $\delta a/a \sim 10^{-5} - 10^{-6}$. For example, the lattice parameters of a diamond plate and large undoped silicon and germanium crystals were determined in [246]. Average values were obtained and their standard deviations were calculated for measurements from eight to twelve reflections for diamond ($a = 3.566986$ Å, $\delta a/a = 2.6\times10^{-6}$), silicon ($a = 5.430941$ Å, $\delta a/a = 2\times10^{-6}$), and germanium ($a = 5.657820$ Å, $\delta a/a = 1.6\times10^{-6}$).

The Renninger method using SR gave important information on lattice parameters for heteroepitaxial $Al_{0.304}Ga_{0.172}In_{0.524}As$ layers grown on InP substrates [247] and on the deformation of an InAs film on GaAs substrates [248, 249]. The authors of [250] studied deformation in a monoclinic MBANP ($C_{13}H_{13}N_3O_2$) crystal caused by an electric field and determined four piezoelectric coefficients.

5. Interference method for determining interplane distances

X-ray interferometry is a comparatively new direction in modern experimental physics. The method has demonstrated unique possibilities in various fields of the study of condensed media: measurements of fundamental physical constants, optical constants in the hard X-ray region ($E = 10-100$ keV), precision measurements of crystal lattice parameters, studies of structural defects in almost perfect single crystals, and X-ray phase-contrast microscopy [251–253].

Fundamental physical constants such as the Avogadro constant, relations between the Planck constant and neutron mass, the wavelengths of characteristic X-ray spectra and γ quanta can be determined using perfect silicon crystals. However, this requires accurate knowledge of the lattice parameter. Because of the relation between fundamental constants and other precisely determined physical constants, the relative accuracy of measuring the Si lattice parameter should be no worse than 10^{-8}, and in some cases (for example, for determining the Avogadro constant [254]) it should approach 10^{-9}.

Hart [225] was one the first to show that a tree-crystal Laue X-ray LLL interferometer is promising for the precision measurement of the interplane distance of a crystal lattice. The interferometer consists of three plates, S, M, and A,

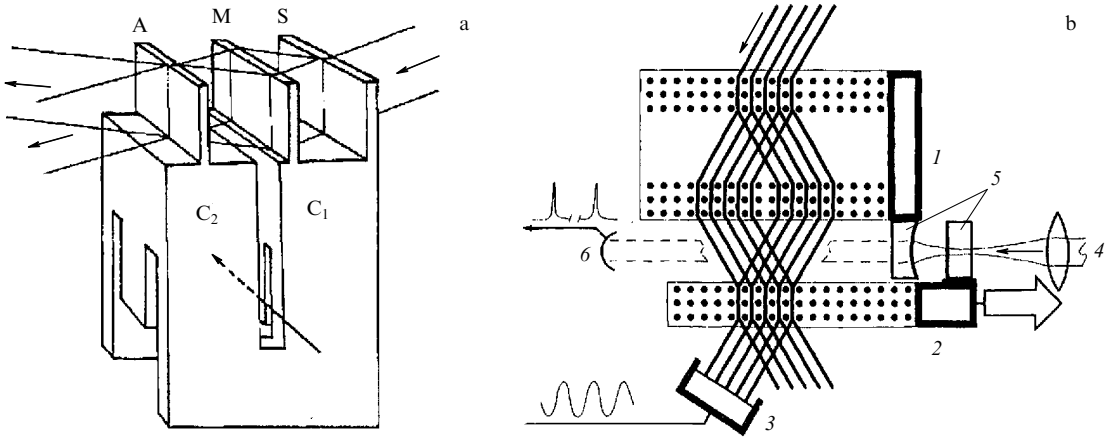

Figure 23. (a) Diagram of a scanning Hart interferometer [251]; S and M are a beam splitter and a mirror in the immobile part C_1 of the interferometer, A is an analyzer in its mobile part C_2 (the arrow shows the load application place). (b) Schematic of an X-ray optical interferometer: *1*, *2* — immobile and mobile parts of the interferometer, respectively; *3* — detector, *4* — laser beam, *5* — mirrors forming an optical Fabry–Perot interferometer, *6* — photoelectronic multiplier [260].

perpendicular to a common base and made of a single crystal silicon block (Fig. 23a). An X-ray beam is incident on a beam-splitter S behind which the transmitted and diffracted beams diffract on a mirror M and overlap on a crystal analyzer A. Their interference gives rise to a standing X-ray wave with a period equal to the interplane distance d. If the interferometer is made of a high-quality single crystal block, X-rays are very weakly absorbed in the crystal analyzer. If the crystal analyzer is displaced with respect to blocks S and M in the direction of the diffraction vector by a distance of $d/2$, the antinodes of the standing wave will 'fall' on the atomic planes of the analyzer, resulting in the strong absorption of radiation. During analyzer scanning in the direction of the diffraction vector, the detector will fix radiation intensity oscillations with period d.

The interferometer described here is an achromatic device, because conditions for the maximum and minimum intensity are independent of the wavelength. This circumstance provided the basis for the assumption that the crystal lattice parameter can be measured by counting the number of bands of the translation moiré per unit length; in this case, knowledge of the X-ray wavelength is not required.

The translation moiré picture in a scanning interferometer [255–257] is obtained by moving the analyzer with respect to a standing wave. The interferometer uses silicon elasticity, required to provide the parallel and rectilinear motion of one crystal part of the interferometer with respect to its immobile part, and is constructed so that its analyzer is connected by two jumpers with a silicon block bearing a beam-splitter and a mirror (Fig. 23a). The scanning interferometer provides excellent stability and ensures the absence of clearance during analyzer displacement.

The absolute measurement accuracy can be improved over that obtained by traditional methods if the radiation wavelength used in experiments is known with a high precision or if a high-quality standard single crystal is grown with very accurately determined interplane distances [258]. These two problems can be solved using a combination of optical and X-ray interferometry. Such an original concept of determining the absolute value of the interplane distance of a crystal lattice directly in units of the standard wavelength of light was proposed and realized in papers [259, 260].

Thanks to a combination of X-ray and optical interferometers, it is possible to measure simultaneously the intensity of X-ray and optical beams during the displacement of the crystal analyzer. One of the two mirrors (*5*) of the optical Fabry–Perot interferometer (Fig. 23b) is attached to the immobile part (*1*), and the second mirror to the mobile part (*2*) of the X-ray interferometer. As a radiation source, a stabilized laser (*4*) is commonly used with the wavelength measured with the relative accuracy of $\sim 10^{-10}$. Thus, the displacement of the crystal analyzer is measured in the optical and X-ray scales, so that the ratio $\lambda/2d$ is expressed via the ratio of the number n of X-ray periods to the number m of optical periods contained in the given scan [261]:

$$d = \frac{m}{n}\frac{\lambda}{2} = \frac{(P+v)\lambda}{2}\,, \tag{38}$$

where P and v are the integer and fractional parts of the ratio m/n.

To avoid counting all moiré bands, it is sufficient to determine the fractional part v at the final stage of the analyzer displacement; the increase in the displacement length (in [262], the progression of 1, 10, 100, 1000, and 5000 optical periods was used) leads to an increase in the experiment accuracy by stages. The fractional part can be calculated by the method of phase steps [263] or quadrature signals [264].

It follows from (38) that, the larger the displacement of the crystal analyzer, the higher the method accuracy. The displacement range is limited by the displacement smoothness and rectilinearity to within a few nanometers. In addition, it is important to preserve the 'pitch' (a turn in the analyzer surface plane) and the 'yaw' (a turn in the diffraction plane) within a few nanoradians over the total scanning length. It is also necessary to provide a good visibility of the moiré picture, demanding a compromise between the opposite requirements of the maximal displacement and the rigidness of the interferometer construction. The construction rigidity is necessary to reduce vibrations impairing the visibility to fractions of an angström.

Progress in X-ray and optical interferometry assumes the development of more powerful methods for more precise control of experimental conditions to increase the displace-

ment range and decrease parasitic rotations and transverse motions.

The increase in the scanning range improves the measurement accuracy and makes possible the study of the larger region of the crystal analyzer, thereby controlling the degree of its perfectness and also measuring the real average value of the lattice parameter. Therefore, it seems that the most promising setup is a separate two-block X-ray interferometer [265] used simultaneously with an optical interferometer [254, 266, 267]. Ensuring its successful operation is not a simple task, because its immobile and mobile parts must be aligned so that vibrations and displacements do not affect the measurement accuracy.

The authors of review [253] have attempted to consider the successive refinements of the method introduced by several research groups, participants in a peculiar scientific relay race, bringing closer the solution to an important metrology problem — the creation of a new standard of length.

In 2011 [268] and 2015 [269], two values of the interplane distance d_{220} in a silicon crystal at 20 °C were obtained: $d_{220} = 1.9201471267(67)$ Å and $d_{220} = 1.9201471198(34)$ Å with a high accuracy ($\delta a/a \approx 3.5 \times 10^{-9}$ and $\delta a/a \approx 1.75 \times 10^{-9}$, respectively). However, it was found later in [270] that, to determine the Avogadro constant correctly, two corrections have to be introduced into these values: into the laser beam diffraction [269] and into the surface strains in the crystal analyzer (sample) [254, 271, 272]. Nevertheless, it seems that the problem of determining the silicon lattice parameter with an accuracy of $\sim 10^{-9}$ can be assumed to be solved.

6. Method of standards

The use of a standard material with known lattice parameters for relative measurements of the lattice parameters of various crystals is undoubtedly an attractive approach, allowing the problem of the uncertainty of the radiation wavelength to be solved. Buschert [273] was the first to apply this approach, which later became widespread [2, 4, 274] due to the use of high-quality standards, for example, silicon and germanium.

When two crystals have different lattice parameters d_A and d_B, detectors register the two-crystal DRC of a crystal standard and a crystal sample at their different angular positions (Fig. 24). In this case, the rotation angle $\Delta\theta$ of the sample is twice as large as the difference between Bragg angles of the two crystals, so that, if $\Delta d = d_A - d_B$ is small, then the angular separation $\Delta\theta$ of peaks is determined by the equation

$$\Delta\theta = 2 \tan\theta \, \frac{\Delta d}{d} \, . \tag{39}$$

Because most of comparative methods determine the difference $\Delta\theta$ in diffraction angles, the exact value of the wavelength is a second-order effect, compared to the difference between angles, only if it is not large [3].

Most of the comparative methods use the Bragg diffraction geometry, which has advantages over the Laue geometry, because measurements can be performed locally, i.e., diffraction parameters are determined by the state of the crystal lattice in a very small region near the crystal surface close to the incident beam.

The method can be used in different forms.

The double-beam method uses the triple reflection scheme to compare lattice parameters using a two-axis diffractometer [276, 277]. A device proposed in [276] consists of a sample and a reference crystal located in the nondispersion diffraction geometry and made of the same material but different in purity (or deformation, stoichiometry, concentration of point defects, etc.). The difference between the Bragg angles of a sample and a reference crystal is measured as the angle between doubly reflected (reference–sample) and triply diffracted (reference–sample–reference) beams. The triple-reflection method using one beam is described in [278].

A modification of the three-crystal method developed by Buschert [273] uses the asymmetric reflection of the first crystal to produce two parallel beams required to obtain simultaneous nondispersion diffraction from the reference crystal and the crystal under study located on the same axis of a goniometer. The beams reflected from these crystals diffract on the third crystal (analyzer) and are registered by detectors. The sample lattice parameter is measured from the angular difference between the positions of diffraction peaks. Such a use of two parallel beams provides a high sensitivity ($\delta d/d \sim 3 \times 10^{-8}$), removes the time delay between measurements of standard and unknown crystals, and considerably reduces problems related to temperature drift and mechanical instability. The method was used to study the influence of isotope concentration on the lattice parameter of perfect germanium crystals [279]. Similar constructions of diffractometers are described in [280–282].

The authors of [275] proposed a method for measuring the difference of lattice parameters for an unknown sample and a standard reference crystal with a relative accuracy of $\sim 10^{-9}$ using two radiation sources to illuminate the same region of the crystal under study and two detectors (see Fig. 24). This experimental setup requires nonstandard equipment, careful alignment for many hours, and a long time to obtain stable conditions for measurements. The last two circumstances probably deterred potential users [4].

A method for determining the lattice parameter using two X-ray beams with different wavelengths was proposed in [283] and [284]. The authors used two characteristic lines, $K\alpha_1$ and $K\beta_1$, and two detectors. In papers [285–287], the CuKα doublet was used. This modification made possible the use of one detector in experiments (Fig. 25a). The lattice parameter was determined by measuring the angular distance between the DRC of the sample and the monochromator used as the reference.

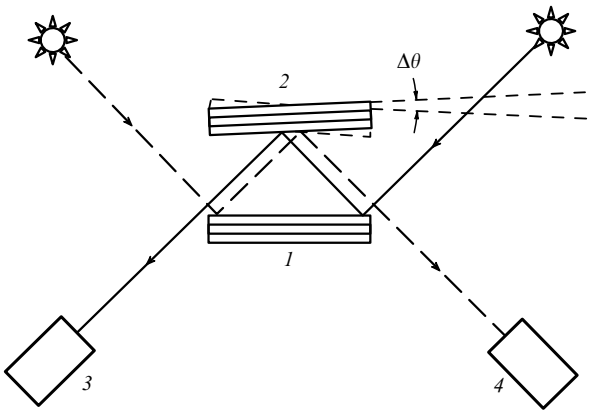

Figure 24. Nondispersion diffractometer with two radiation sources and two detectors: *1* — reference crystal, *2* — crystal under study, *3* and *4* — detectors [275].

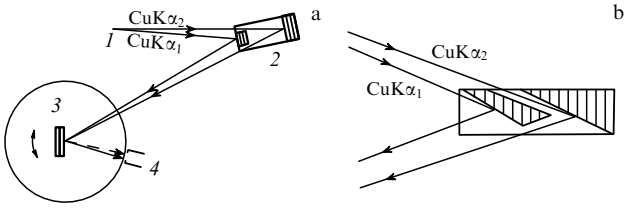

Figure 25. (a) Schematic of experiments on the relative determination of the GaAs lattice parameter using the CuKα spectral doublet: *1* — radiation source, *2* — germanium monochromator (reference), *3* — GaAs sample [285]. (b) Improved construction of a germanium monochromator [286].

The GaAs crystal parameter was determined in [286] using a Ge crystal monochromator with the lattice parameter close to that of GaAs. To obtain low-divergent beams at the monochromator output, its working surfaces were inclined to the (444) diffraction surface so that the grazing angle of the first beam was equal to 5° (Fig. 25b). The accuracy of measuring the lattice parameter was $\delta a = 4 \times 10^{-5}$ Å, corresponding to $\delta a/a \sim 7 \times 10^{-6}$. The authors of [287], using a device for precise positioning of crystals and a proportional position-sensitive detector, managed to improve the accuracy and to achieve the value $\delta a/a \sim 10^{-7}$.

If the distribution of impurities in a crystal is homogeneous, the relaxation of the inner stress appears near the surface. Therefore, in experiments with Bragg diffraction schemes, deformations related to surface effects should be well known. After cutting an appropriate silicon plate, the crystal surface should be polished very carefully.

When the Laue geometry is used, the influence of surface damages, which cannot be removed completely by etching and polishing, is negligibly small, and the interplane distance, unlike the Bragg geometry, is mainly determined not in the surface layer of the crystal but in its volume. This explains the appearance of many studies devoted to measurements of the lattice parameter using nondispersion diffraction schemes in the Laue geometry [258, 274, 288–296].

In [290], an MoKα$_1$ radiation beam (*1*) (Fig. 26a) formed in a monochromator was directed on a crystal (*2*) under study. The transmitted and reflected beams diffract on a third (reference) crystal (*3*), and the intensities of the TR (transmitted and diffracted) and RR (doubly diffracted) beams are measured by two independent detectors D_{TR} and D_{RR}. In all crystals, the symmetric Mo(220) reflection is used. A relative accuracy of 2×10^{-7} was achieved.

In 1994, the NIST (National Institute of Standards and Technology, USA) system was developed for the relative determination of the lattice parameter [291, 292, 294–296]. The NIST comparator uses the symmetric two-crystal nondispersion diffraction in the Laue geometry proposed by Hart [274] and improved in papers [258, 288, 289]. The NIST comparator, shown schematically in Fig. 26b, has several features improving the accuracy of measuring the lattice parameter. The comparator includes two radiation sources, S_1 and S_2, gates (*4*), and two detectors, D_1 and D_2. X-ray sources are located with respect to the first (reference) crystal (*2*) so that the crystal reflects the beams coming from both sources simultaneously. By rotating the second crystal (sample) (*1*), a two-crystal rocking curve is recorded in turn by the first and second detector. Gates make possible the recording of doubly diffracted DRCs from one source without interference of singly diffracted beams emitted by another source. The two-crystal DRCs of almost the same thickness have the fine structure [297] (Fig. 26c) — thickness oscillations (Pendellösung) — which can be easily used to determine the DRC position with improved accuracy. The typical accuracy of the relative determination of the interplane distance is $(5-10) \times 10^{-9}$; it includes the statistic contribution $((3-9) \times 10^{-9})$ and three systematic components: the crystal temperature (from 3×10^{-9}), the alignment of crystals (1×10^{-9}), and the localization of crystals and X-ray trajectories (3×10^{-9}) [296].

The NIST comparator has played an important role in the International Avogadro Project [293, 298] and in the determination of the absolute value of the lattice parameter of silicon single crystals used for manufacturing standard powder diffraction materials [293]. It also helped to find a small but considerable sensitivity of the lattice period to the method of preparation of the surface of crystals under study, although measurements were performed in the symmetric Laue geometry [293].

7. Conclusions

This review has shown that a variety of methods exist for high-precision measuring of crystal lattice parameters using Bragg reflections. In most cases, an appropriate method depends on the material type and the goal of the studies.

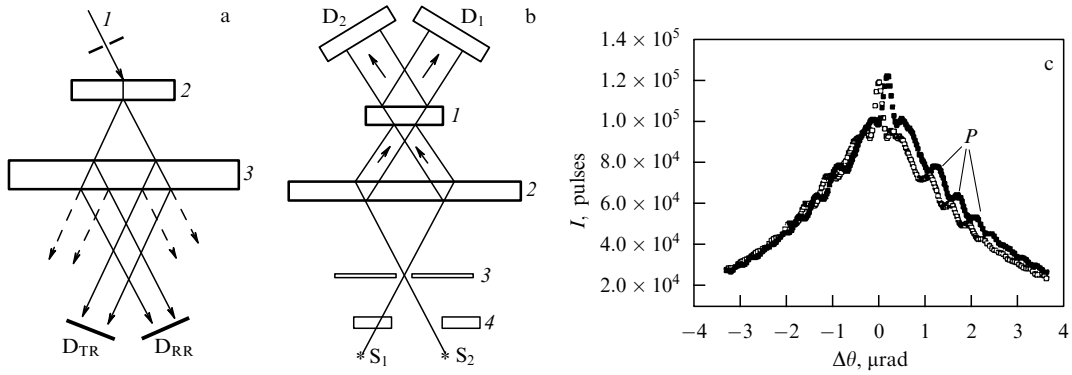

Figure 26. Diagrams of double-crystal diffractometers using nondispersion symmetric Laue diffraction. (a) *1* — monochromatic X-ray beam, *2* — sample, *3* — reference crystal, D_{TR} and D_{RR} are detectors recording the transmitted-diffracted and double-diffracted beams, respectively [290]; (b) S_1 and S_2 are radiation sources, *1* — sample, *2* — reference crystal, D_1 and D_2 are detectors, *3* — slit, *4* — gates; (c) two DRCs (the (440) reflection of silicon) registered by detectors D_1 and D_2 (*P* is thickness oscillations) [295] (see text).

The most widespread method for measuring the absolute value of the lattice parameter of single crystals is the Bond method. This method reliably provides a relative accuracy of $10^{-5}-10^{-6}$. The method removes problems related to the inaccurate alignment of a sample and a goniometer with respect to the incident beam, because it requires measurements of only the relative angular positions of a sample. Therefore, the error in the angular position of a detector does not matter. The inaccurate alignment of the sample with respect to the goniometer axis results in the displacement of only the position of the diffracted beam, but not the angle at which the beam diffracts. However, in this case, a problem exists for inhomogeneous or deformed samples, because the incident beam will illuminate different regions of a crystal in its two positions, which will produce an error in the determination of the lattice parameter. In addition, problems can appear when measuring all lattice parameters of noncubic crystals. In such cases, it is necessary to prepare several samples or to use a special approach to solving the problem.

The Kossel projection method is a powerful tool for studying the structural features of a broad class of crystalline objects. This is an unsurpassable method of X-ray microdiffraction combining good locality, precision, and informativity. It seems that this method can be characterized by the principle 'everything at once,' because diffractograms contain many lines corresponding to different resolved reflections satisfying the geometrical conditions of the experiment. This circumstance advantageously distinguishes the Kossel projection method from other known X-ray diffraction methods and opens up the possibility of real-time studies of the different anisotropic states of a crystal lattice (*in situ* studies).

The further development of experimental equipment (improving the resolution of CCD detectors, improving X-ray optics, etc.) opens up wide possibilities for using the Kossel projection method to study fast processes, investigate nanoobjects, and rapidly analyze crystals. An especially interesting possibility is the focusing of an intense SR beam onto a micrometer spot, which, for example, can be used for precise measurements of deformation in individual crystallites of large-grain materials. Due to the use of modern third- and fourth-generation synchrotron sources and digital image processing, the Kossel method can soon experience a renaissance of high-precision determining of lattice parameters and studying the perfection of crystals.

Similarly to the Kossel projection method, the Renninger method can also be used to measure many reflections and to measure all the lattice parameters, rather than only one, as in the Bond method. The Renninger method allows one to minimize errors caused by absorption, sample displacement, the inaccuracy in angular positions measured with a detector, and other systematic errors inherent in most methods of determining lattice parameters.

The Renninger method has an 'internal' criterion for sample adjustment, because the adjustment is performed upon azimuthal rotation of a single crystal around the diffraction vector of the first reflection. Obviously, this method is one of the most efficient and informative for determining lattice deformation and constructing the deformation tensor. A disadvantage of the method at present is the complex interpretation (indexing) of multiwave diffraction patterns, and for this reason it is less popular than the Bond method.

High-resolution Bragg diffraction upon backscattering was successfully used to measure lattice parameters and X-ray wavelengths with a high relative accuracy of $(10^{-6}-10^{-8})$. However, this method is not widely used because of its complicated equipment.

The comparative precision determination of the lattice parameter with a relative accuracy of $10^{-8}-10^{-9}$ was performed by the method of two coplanar reflections and the reference method. Measurements performed by these methods allow one to estimate variations in the lattice parameter of almost ideal zone-melting commercial silicon between individual ingots and within a particular ingot. In particular, such measurements are necessary for the preliminary characterization of the homogeneity of materials used to fabricate reference crystals.

This work was supported by the Ministry of Science and Higher Education within the framework of the State Project of the Federal Scientific Research Center Crystallography and Photonics of the RAS.

References

1. Schwarzenbach D et al. *Acta Cryst. A* **45** 63 (1989)
2. Hart M *J. Cryst. Growth* **55** 409 (1981)
3. Fewster P F *J. Mater. Sci. Mater. Electron.* **10** 175 (1999)
4. Galdecka E, in *International Tables for Crystallography* Vol. C (New York: Wiley, 2006) p. 505
5. Lisoivan V I *Izmereniya Parametrov Elementarnoi Yacheiki na Odnokristal'nom Spektrometre* (Measurements of Unit Cell Parameters with a Single-Crystal Spectrometer) (Novosibirsk: Nauka, 1982)
6. Kossel W, Loeck V, Voges H *Z. Phys.* **94** 139 (1935)
7. Kossel W *Gött. Nachr. Math. Naturwiss.* **1** 229 (1935)
8. Kossel W, Voges H *Ann. Physik* **23** 677 (1935)
9. Kossel W *Ann. Physik* **25** 512 (1936)
10. Lonsdale K *Philos. Trans. R. Soc. Lond. A* **240** 219 (1947)
11. Yakowitz H *J. Appl. Phys.* **37** 4455 (1966)
12. Tixier R, Waché C *J. Appl. Cryst.* **3** 466 (1970)
13. Aristov V V, Shekhtman V Sh, Shmyt'ko I M *Sov. Phys. Crystallogr.* **18** 445 (1973); *Kristallogr.* **18** 706 (1973)
14. Pekarev A I, Chistyakov Yu D *Zavod. Labor.* **35** 1075 (1969)
15. Dingley D J *Scanning* **1** 79 (1978)
16. Langer E, Däbritz S *IOP Conf. Ser. Mater. Sci. Eng.* **7** 012015 (2010)
17. Lider V V *Crystallogr. Rep.* **56** 169 (2011); *Kristallogr.* **56** 196 (2011)
18. Borrmann G *Naturwissenschaften* **23** 591 (1935)
19. Borrmann G *Ann. Physik* **27** 669 (1936)
20. Isherwood B J, Wallace C A *Nature* **212** 173 (1966)
21. Lamaze J P, Despujols J *J. Phys. E* **9** 41 (1976)
22. Castaing R, Ph.D. Thesis (Paris: Univ. de Paris, 1951)
23. Castaing R, Guinier A *C.R. Acad. Sci. Paris* **232** 1948 (1951)
24. Yakowitz H *The Divergent Beam* (*Kossel*) *X-Ray Method and Its Uses in Measuring Strain Contours in an Individual Grain of Fe-3 Weight Percent Si Transformer Sheet* (Washington, DC: National Bureau of Standards, 1973)
25. Frazer J Z, Keil K, Reid A M *Am. Mineral.* **54** 554 (1969)
26. Dingley D J, Ferran G *Micron* **8** 145 (1977)
27. Langer E et al. *Appl. Surf. Sci.* **179** 45 (2001)
28. Böhling M, Bauch J *Cryst. Res. Technol.* **42** 905 (2007)
29. Bouscaud D et al. *Ultramicroscopy* **115** 115 (2012)
30. Umeno M, Kawabe H, Shinoda G *Adv. X-Ray Anal.* **9** 23 (1966)
31. Mendelssohn M J, Milledge H J *Acta Cryst. A* **55** 204 (1999)
32. Lider V V, Rozhanskii V N *Fiz. Tverd. Tela* **9** 3541 (1967)
33. Hejna J et al. *Scanning* **8** 177 (1986)
34. Ullrich H-J et al. *Mikrochim. Acta* **107** 283 (1992)
35. Däbritz S, Langer E, Hauffe W *J. Anal. At. Spectrom.* **14** 409 (1999)
36. Nikl M *Meas. Sci. Technol.* **17** R37 (2006)
37. Ullrich H *Mikrochim. Acta* **101** 19 (1990)
38. Berveiller S et al. *Mater. Sci. Forum* **490–491** 159 (2005)
39. Lider V V, Chukhovskii F N, Rozhanskii V N *Sov. Phys. Solid State* **19** 816 (1977); *Fiz. Tverd. Tela* **19** 1231 (1977)
40. Hanneman R E, Ogilvie R E, Modrzejewski A *J. Appl. Phys.* **33** 1429 (1962)
41. Kumakhov M A *X-Ray Spectrom.* **29** 343 (2000)

42. MacDonald C A *X-Ray Opt. Instrum.* **2010** 1 (2010)
43. Ternov I M, Mikhailin V V *Sinkhrotronnoe Izluchenie. Teoriya i Eksperiment* (Synchrotron Radiation. Theory and Experiment) (Moscow: Energoatomizdat, 1986)
44. Langer E et al. *Appl. Surf. Sci.* **252** 240 (2005)
45. Langer E, Haschke M, Däbritz S *Microchim. Acta* **161** 455 (2008)
46. Bortel G et al. *J. Synchrotron Rad.* **23** 214 (2016)
47. Ullrich H-J, Schlaubitz M, Friedel F *Nucl. Instrum. Meth. Phys. Res. A* **349** 269 (1994)
48. Bauch J et al. *Cryst. Res. Technol.* **34** 71 (1999)
49. Schetelich Ch, Brenner S, Geist V *J. Synchrotron Rad.* **5** 102 (1998)
50. Schetelich Ch et al. *Nucl. Instrum. Meth. Phys. Res. B* **103** 236 (1995)
51. Glazer A M et al. *J. Synchrotron Radiat.* **11** 187 (2004)
52. Glazer A M *Philos. Trans. R. Soc. Lond. A* **373** 20140232 (2015)
53. Bearden J A *Rev. Mod. Phys.* **39** 78 (1967)
54. Cohen E R, Taylor B N *J. Res. Natl. Bureau Stand.* **92** 85 (1987)
55. Ullrich H-J et al. *Krist. Tech.* **7** 1153 (1972)
56. Harris N *J. Mater. Sci.* **10** 279 (1975)
57. Weber S, Schetelich Ch, Geist V *Cryst. Res. Technol.* **29** 727 (1994)
58. Weber S *J. Appl. Cryst.* **30** 85 (1997)
59. Langer E, Kurt R, Daebritz S *Cryst. Res. Technol.* **34** 801 (1999)
60. Maurice C, Fortunier R J *Microscopy* **230** 520 (2008)
61. Gielen P et al. *J. Appl. Phys.* **36** 773 (1965)
62. Heise B H *J. Appl. Phys.* **33** 697 (1962)
63. Morris W G *J. Appl. Phys.* **39** 1813 (1968)
64. Harris N, Kirkham A J *J. Appl. Cryst.* **4** 232 (1971)
65. Biggin S, Dingley D J *J. Appl. Cryst.* **10** 376 (1977)
66. Brechbühl J, Bauch J, Ullrich H-J *Cryst. Res. Technol.* **34** 59 (1999)
67. Heise H *J. Appl. Phys.* **33** 938 (1962)
68. Lutts A, Gielen P J *J. Appl. Cryst.* **4** 242 (1971)
69. Spooner F J, Wilson C G *J. Appl. Cryst.* **6** 132 (1973)
70. Isherwood B J *J. Appl. Cryst.* **1** 299 (1968)
71. Isherwood B J, Wallace C A *Acta Cryst. A* **27** 119 (1971)
72. Isherwood B J, Brown B R, Halliwell M A *J. Cryst. Growth* **54** 449 (1981)
73. Isherwood B J, Brown B R, Halliwell M A *J. Cryst. Growth* **60** 33 (1982)
74. Glass H L, Moudi L A *J. Appl. Cryst.* **7** 22 (1974)
75. Yakowitz H *J. Appl. Phys.* **43** 4793 (1972)
76. Morawiec A, Pesci R, Lecomte J S *Ceram. Trans.* **201** 163 (2008)
77. Morawiec A *J. Appl. Cryst.* **49** 322 (2016)
78. Bouscaud D et al. *J. Appl. Cryst.* **47** 1699 (2014)
79. Shekhtman V Sh et al. *Dokl. Akad. Nauk SSSR* **205** 834 (1972)
80. Newman B A *J. Appl. Cryst.* **3** 191 (1970)
81. Imura T, Weissmann S, Slade J J (Jr.) *Acta Cryst.* **15** 786 (1962)
82. Berg H M, Hall E L *Adv. X-Ray Anal.* **18** 454 (1975)
83. Ellis T et al. *J. Appl. Phys.* **35** 3364 (1964)
84. Kalman Z H et al. *Metall. Trans. A* **19** 217 (1988)
85. Newman B A, Weissmann S *J. Appl. Cryst.* **1** 139 (1968)
86. Newman B A, Shrier A *J. Appl. Cryst.* **3** 280 (1970)
87. Koishi Y, Gillies D C *Am. Mineral.* **64** 211 (1979)
88. Aristov V V, Shmytko I M *J. Appl. Cryst.* **11** 662 (1978)
89. Lin A L, Donaghey L F *J. Electron. Mater.* **6** 383 (1977)
90. Lider V V "Novye vozmozhnosti primeneniya difraktsii shiroko raskhodyashchegosya puchka rentgenovskikh luchei" ("New possibilities of application of a widely divergent X-ray beam"), PhD Thesis (Phys.-Math) (Moscow: Shubnikov Institute of Crystallography, AN SSSR, 1977)
91. Pinsker Z G *Dinamicheskoe Rasseyanie Rentgenovskikh Luchei v Ideal'nykh Kristallakh* (Dynamic Scattering of X-Rays in Ideal Crystals) (Moscow: Nauka, 1974)
92. James R W *The Optical Principles of the Diffraction of X-Rays* (London: Bell, 1967); Translated into Russian: *Opticheskie Printsipy Difraktsii Rentgenovskikh Luchei* (Moscow: IL, 1950)
93. Lutts A *J. Appl. Cryst.* **6** 428 (1973)
94. Bond W L *Acta Cryst.* **13** 814 (1960)
95. Baker T W et al. *Adv. X-Ray Anal.* **11** 359 (1968)
96. Segmuller A *Adv. X-Ray Anal.* **13** 455 (1970)
97. Godwod K, Kowalczyk R, Szmid Z *Phys. Status Solidi A* **21** 227 (1974)
98. Hubbard C R, Mauer F A *J. Appl. Cryst.* **9** 1 (1976)
99. Lukaszewicz K et al. *Krist. Tech.* **13** 561 (1978)
100. Bartels W J *J. Vac. Sci. Technol. B* **1** 338 (1983)
101. Grosswig S et al. *Cryst. Res. Technol.* **18** 501 (1983)
102. Schmidbauer M, Kwasniewski A, Schwarzkopf J *Acta Cryst. B* **68** 8 (2012)
103. Shikata S et al. *Jpn. J. Appl. Phys.* **57** 111301 (2018)
104. Willoughby A F W, Driscoll C M H, Bellamy B A *J. Mater. Sci.* **6** 1389 (1971)
105. Nakajima M et al. *Appl. Phys. Lett.* **49** 1251 (1986)
106. Usuda K et al. *Jpn. J. Appl. Phys.* **29** L210 (1990)
107. Chen N F et al. *Rigaku J.* **13** 16 (1996)
108. Wokulska K et al. *Solid State Phenom.* **163** 264 (2010)
109. Paszkowski R et al. *Cryst. Res. Technol.* **48** 413 (2013)
110. Paszkowski R, Wokulska K, Dec J *Cryst. Res. Technol.* **52** 1600368 (2017)
111. Kucharczyk D, Niklewski T *J. Appl. Cryst.* **12** 370 (1979)
112. Ridou C, Rousseau M, Freund A *J. Phys. Lett.* **38** 359 (1977)
113. Horváth J, Kucharczyk D *Phys. Status Solidi A* **63** 687 (1981)
114. Pietraszko A et al. *Phase Transit.* **1** 99 (1979)
115. Pietraszko A, Tomaszewski P E, Lukaszewicz K *Phase Transit.* **2** 131 (1981)
116. Okada Y, Tokumaru Y *J. Appl. Phys.* **56** 314 (1984)
117. Bublik V T, Konyaeva E P, Smirnov I S *Zavod. Labor.* **42** 284 (1976)
118. Bublik V T, Wilke J, Pereversev A *Phys. Status Solidi A* **73** K271 (1982)
119. Ono F, Maeta H *J. Phys. Colloq.* **49** C8-63 (1988)
120. Haruna K et al. *Jpn. J. Appl. Phys.* **31** 2527(1992)
121. Saotome T et al. *J. Phys. Condens. Matter* **10** 1267 (1998)
122. Giles C et al. *J. Synchrotron Rad.* **12** 349 (2005)
123. Ratuszna A et al. *Phys. Status Solidi A* **54** 739 (1979)
124. Kucharczyk D, Pietraszko A, Lukaszewicz K *Phys. Status Solidi A* **37** 287 (1976)
125. Åsbrink S, Wolcyrz M, Hong S-H *Phys. Status Solidi A* **87** 135 (1985)
126. Okada Y, Tokumaru Y, Kadota Y *Appl. Phys. Lett.* **48** 975 (1986)
127. Yasuami S et al. *J. Cryst. Growth* **100** 600 (1990)
128. Usuda K, Ando M *J. Appl. Phys.* **80** 1352 (1996)
129. Grosswig S, Härtwig J, Schellenberger U *Phys. Status Solidi A* **76** 241 (1983)
130. Dressler L, Griebner U, Kittner R *Cryst. Res. Technol.* **22** 1431 (1987)
131. Morozov A N, Bublik V T *J. Cryst. Growth* **75** 491 (1986)
132. Morozov A N et al. *Crystallogr. Rep.* **28** 458 (1983); *Kristallogr.* **28** 776 (1983)
133. Morozov A N, Abaeva T V, Bublik V T *Cryst. Res. Technol.* **21** 613 (1986)
134. Bublik V T et al. *Izv. Akad. Nauk SSSR. Neorg. Mater.* **20** 364 (1984)
135. Boiko V M et al. *Semiconductors* **40** 749 (2006); *Fiz. Tekh. Poluprovodn.* **40** 769 (2006)
136. Bublik V F et al. *Sov. Phys. Crystallogr.* **18** 218 (1973); *Kristallogr.* **18** 353 (1973)
137. Anastas'eva N A et al. *Crystallogr. Rep.* **23** 174 (1978); *Kristallogr.* **23** 314 (1978)
138. Aref'ev I S et al. *Crystallogr. Rep.* **32** 267 (1987); *Kristallogr.* **32** 460 (1987)
139. Pillukat A, Karsten K, Ehrhart P *Phys. Rev. B* **53** 7823 (1996)
140. Karsten K, Ehrhart P *Phys. Rev. B* **51** 10508 (1995)
141. Boiko V M et al. *Semiconductors* **40** 621 (2006); *Fiz. Tekh. Poluprovodn.* **40** 641 (2006)
142. Bublik V F et al. *Crystallogr. Rep.* **22** 705 (1977); *Kristallogr.* **22** 1240 (1977)
143. Morozov A N, Bublik V F, Kovalchuk I A *Crystallogr. Rep.* **31** 586 (1986); *Kristallogr.* **31** 986 (1986)
144. Gaber A et al. *J. Appl. Phys.* **82** 5348 (1997)
145. Mullin J B et al. *J. Appl. Phys.* **47** 2584 (1976)
146. Gaidai L I et al. *Elektron. Tekh. Ser. 6* **2** 84 (1979)
147. Wilke J et al. *Cryst. Res. Technol.* **18** 787 (1983)
148. Bublik V F et al. *Crystallogr. Rep.* **27** 621 (1982); *Kristallogr.* **27** 1084 (1982)
149. Celotti G, Nobili D, Ostoja P *J. Mater. Sci.* **9** 821 (1974)
150. Wolcyrz M, Lukaszewicz K *J. Appl. Cryst.* **15** 406 (1982)
151. Kucytowski J, Wokulska K *Cryst. Res. Technol.* **40** 424 (2005)
152. Lefeld-Sosnowska M et al. *J. Phys. D* **34** A144 (2001)
153. Fewster P F, Willoughby A F W *J. Cryst. Growth* **50** 648 (1980)
154. Fujii K, Okada Y, Orito F *J. Appl. Phys.* **73** 88 (1993)

155. Kucytowski J, Wokulska K, Kazmierczak-Balata A *Thin Solid Films* **516** 8125 (2008)
156. Kazmierczak-Balata A et al. *J. Alloys Comp.* **481** 622 (2009)
157. Grosswig S et al. *Cryst. Res. Technol.* **18** K28 (1983)
158. Pihl C F, Bieber R L, Schwuttke G H *Phys. Status Solidi A* **17** 359 (1973)
159. Baker T W et al. *Nature* **210** 720 (1966)
160. Baker T W et al., AERE-R 5152, Atomic Energy Res. Establ., Harwell (Berkshire) (1969)
161. Burke J, Tomkeieff M V *Acta Cryst. A* **24** 683 (1968)
162. Burke J, Tomkeieff M V *J. Appl. Cryst.* **2** 247 (1969)
163. Gruber E E, Black R E *J. Appl. Cryst.* **3** 354 (1970)
164. Filscher G, Unangst D *Krist. Tech.* **15** 955 (1980)
165. Bradaczek H, Leps B, Uebach W *Z. Naturforsch. A* **37** 448 (1982)
166. Nemiroff M *J. Appl. Cryst.* **15** 375 (1982)
167. Berger H *J. Appl. Cryst.* **19** 34 (1986)
168. Grosswig S, Jäckel K-H, Kittner R *Cryst. Res. Technol.* **21** 133 (1986)
169. Hartwig J, Grosswig S *Phys. Status Solidi A* **115** 369 (1989)
170. Galdecka E *Acta Cryst. A* **49** 106 (1993)
171. Galdecka E *Acta Cryst. A* **49** 116 (1993)
172. Mil'vidskii A M *Metody Issledovaniya Struktur Kristallov. Fazovyi Analiz i Pretsizionnye Izmereniya Parametra Reshetki. Lab. Praktikum* (Methods of Studying the Structure of Crystals. Phase Analysis and Precision Measurements of the Lattice Parameter. Lab. Workshop) (Moscow: Ucheba MISiS, 2005)
173. Härtwig J et al. *Phys. Status Solidi A* **125** 79 (1991)
174. Shvyd'ko Yu V et al. *Phys. Rev. Lett.* **85** 495 (2000)
175. Pacek P et al. *Solid State Phenom.* **130** 73 (2007)
176. Paszkowski R et al. *J. Cryst. Growth* **401** 327 (2014)
177. Bowen D K, Tanner B K *High Resolution X-Ray Diffractometry and Topography* (London: Taylor and Francis, 1998); Translated into Russian: *Vysokorazreshayushchaya Rentgenovskaya Difraktometriya i Topografiya* (St. Petersburg: Nauka, 2002)
178. Lider V V *Zavod. Labor.* **74** 31 (2008)
179. Nakayama K et al. *Z. Naturforsch. A* **28** 632 (1973)
180. Zhang X et al. *J. Appl. Crystallogr.* **36** 188 (2003)
181. Blokhin M A, Shveitser I G *Rentgenospektral'nyi Spravochnik* (X-Ray Spectral Handbook) (Moscow: Nauka, 1982)
182. Ando M et al. *Rev. Sci. Instrum.* **60** 2410 (1989)
183. Usuda K et al. *J. Appl. Phys.* **69** 182 (1991)
184. Okada Y et al. *Nucl. Instrum. Meth. Phys. Res. A* **467–468** 1037 (2001)
185. Obaidur R M *J. Synchrotron Radiat.* **9** 28 (2002)
186. Berger H *J. Appl. Cryst.* **17** 451 (1984)
187. Soller W *Phys. Rev.* **24** 158 (1924)
188. Berger H, Christ B, Troschke J *Cryst. Res. Technol.* **17** 1233 (1982)
189. Härtwig J et al. *Phys. Status Solidi A* **142** 19 (1994)
190. Fewster P F *J. Appl. Cryst.* **22** 64 (1989)
191. Fewster P F, Andrew N L *J. Appl. Cryst.* **28** 451 (1995)
192. Fewster P F, Andrew N L *J. Phys. D* **28** A97 (1995)
193. Fatemi M *Acta Cryst. A* **61** 301 (2005)
194. Kohra K, Matsushita T *Z. Naturforsch. A* **27** 484 (1972)
195. Shvyd'ko Y "X-ray resonators and other applications of Bragg backscattering", Report DESY-THESIS-2002-028 (Hamburg: DESY, 2002) https://doi.org/10.3204/DESY-THESIS-2002-028
196. Shvyd'ko Yu *X-Ray Optics. High-Energy-Resolution Applications* (Berlin: Springer, 2004)
197. Lider V V *Crystallogr. Rep.* **57** 628 (2012); *Kristallogr.* **57** 705 (2012)
198. Sykora B, Peisl H *Z. Angew. Phys.* **30** 320 (1970)
199. Bottom V E, Carvalho R A *Rev. Sci. Instrum.* **42** 196 (1971)
200. Freund A, Schneider J *J. Cryst. Growth* **13–14** 247 (1972)
201. Okazaki A, Kawaminami M *Jpn. J. Appl. Phys.* **12** 783 (1973)
202. Okazaki A, Ohama N *J. Appl. Cryst.* **12** 450 (1979)
203. Ohama N, Sakashita H, Okazaki A *J. Appl. Cryst.* **12** 455 (1979)
204. Okazaki A, Soejima Y *Acta Cryst. A* **57** 708 (2001)
205. Munakata K, Okazaki A *Acta Cryst. A* **60** 33 (2004)
206. Sakashita H, Ohama N, Okazak A *J. Phys. Soc. Jpn.* **50** 4013 (1981)
207. Ohama N, Sakashita H, Okazaki A *Phase Transit.* **4** 81 (1984)
208. Sato M et al. *Phase Transit.* **5** 207 (1985)
209. Soejima Y et al. *Z. Kristallogr.* **195** 161 (1991)
210. Tomonaga N, Soejima Y, Okazaki A *Phase Transit.* **28** 51 (1990)
211. Onitsuka H et al. *Phase Transit.* **47** 93 (1994)
212. Kohno A et al. *Nuovo Cimento D* **19** 293 (1997)
213. Stetsko Yu P, Kshevetskii S A, Mikhailyuk I P *Sov. Tech. Phys. Lett.* **14** 13 (1988); *Pis'ma Zh. Tekh. Fiz.* **14** 29 (1988)
214. Shvyd'ko Y V et al. *J. Synchrotron Radiat.* **9** 17 (2002)
215. Lucht M et al. *J. Appl. Cryst.* **36** 1075 (2003)
216. Hastings J B et al. *Phys. Rev. Lett.* **66** 770 (1991)
217. Shvyd'ko Yu V et al. *JETP Lett.* **53** 69 (1991); *Pis'ma Zh. Eksp. Teor. Fiz.* **53** 69 (1991)
218. Baron A Q R *Hyperfine Interact.* **125** 29 (2000)
219. Wille H-C et al. *Phys. Rev. Lett.* **89** 285901 (2002)
220. Hu M Y et al. *Phys. Rev. B* **67** 113306 (2003)
221. Stoupin S, Shvyd'ko Yu V *Phys. Rev. Lett.* **104** 085901 (2010)
222. Stoupin S, Shvyd'ko Yu V *Phys. Rev. B* **83** 104102 (2011)
223. Mohr P J, Taylor B N *Rev. Mod. Phys.* **72** 351 (2000)
224. Toellner T S *Hyperfine Interact.* **125** 3 (2000)
225. Toellner T S, Alatas A, Said A H *J. Synchrotron Radiat.* **18** 605 (2011)
226. Isomae S et al. *J. Appl. Cryst.* **9** 342 (1976)
227. Lider V V *Crystallogr. Rep.* **39** 352 (1994); *Kristallogr.* **39** 406 (1994)
228. Zozulya A V, Lider V V, Koval'chuk M V *Poverkhnost'. Rentgen. Sinkhrotron. Neitron. Issled.* (12) 28 (2002)
229. Blagov A E et al. *Crystallogr. Rep.* **55** 1074 (2010); *Kristallogr.* **55** 1133 (2010)
230. Zhang X et al. *AIP Conf. Proc.* **1234** 895 (2010)
231. Fujimoto H, Waseda A, Zhang X W *Metrologia* **48** S55 (2011)
232. Waseda A et al. *IEEE Trans. Instrum. Meas.* **64** 1692 (2015)
233. Waseda A et al. *IEEE Trans. Instrum. Meas.* **66** 1304 (2017)
234. Yang J et al. *AIP Conf. Proc.* **2054** 060016 (2019)
235. Terminasov Yu S, Tuzov L V *Sov. Phys. Usp.* **7** 434 (1964); *Usp. Fiz. Nauk* **83** 223 (1964)
236. Chang S-L *Multiple Diffraction of X-Rays in Crystals* (Berlin: Springer-Verlag, 1984); Translated into Russian: *Mnogovolnovaya Difraktsiya Rentgenovskikh Luchei v Kristallakh* (Moscow: Mir, 1987)
237. Yang C-Z, Hao J-M, Pei G-W *Rigaku J.* **17** 46 (2000)
238. Renninger M *Z. Phys.* **106** 141 (1937)
239. Cole H, Chambers F H, Dunn H M *Acta Cryst.* **15** 138 (1962)
240. Post B *J. Appl. Cryst.* **8** 452 (1975)
241. Rossmanith E *J. Appl. Cryst.* **32** 355 (1999)
242. Rossmanith E *J. Appl. Cryst.* **36** 1467 (2003)
243. Kshevetskii S A et al. *Ukr. Fiz. Zh.* **24** 1480 (1979)
244. Kshevetskii S A et al. *Ukr. Fiz. Zh.* **30** 1843 (1985)
245. Borcha M et al. *Proc. SPIE* **7008** 700819 (2008)
246. Hom T, Kiszenik W, Post B *J. Appl. Cryst.* 8 457 (1975)
247. Sasaki J M et al. *J. Cryst. Growth* **172** 284 (1997)
248. Morelhão S L et al. *Microelectron. J.* **36** 219 (2005)
249. Freitas R O et al. *Phys. Status Solidi A* **204** 2548 (2007)
250. Avanci L H et al. *Phys. Rev. B* **61** 6507 (2000)
251. Hart M *Proc. R. Soc. Lond. A* **346** 1 (1975)
252. Siddons D P *AIP Conf. Proc.* **75** 236 (1981)
253. Lider V V *Phys. Usp.* **57** 1099 (2014); *Usp. Fiz. Nauk* **184** 1217 (2014)
254. Cavagnero G et al. *Metrologia* **41** 56 (2004)
255. Hart M *Brit. J. Appl. Phys.* **1** 1405 (1968)
256. Hart M, Siddons D P *Proc. R. Soc. Lond. A* **376** 465 (1980)
257. Bonse U, Lotsch H, Henning A *J. X-Ray Sci. Technol.* **1** 107 (1989)
258. Baker J F C, Hart M *Acta Cryst. A* **31** 364 (1975)
259. Deslattes R D *Appl. Phys. Lett.* **15** 386 (1969)
260. Deslattes R D, Henins A *Phys. Rev. Lett.* **31** 972 (1973)
261. Basile G et al. *IEEE Trans. Instrum. Meas.* **38** 210 (1989)
262. Bergamin A et al. *Eur. Phys. J. B* **9** 225 (1999)
263. Schwarzenberger D R, Chetwynd D G, Bowen D K *J. X-Ray Sci. Technol.* **1** 134 (1989)
264. Yacoot A, Kuetgens U *Meas. Sci. Technol.* **23** 074003 (2012)
265. Bonse U, te Kaat E *Z. Phys.* **214** 16 (1968)
266. Becker P, Mana G *Metrologia* **31** 203 (1994)
267. Ferroglio L, Mana G, Massa E *Opt. Express* **16** 16877 (2008)
268. Massa E et al. *Metrologia* **48** S37 (2011)
269. Massa E et al. *J. Phys. Chem. Ref. Data* **44** 031208 (2015)
270. Fujii K et al. *Metrologia* **55** L1 (2018)
271. Quagliotti D et al. *Metrologia* **50** 243 (2013)
272. Melis C et al. *Metrologia* **53** 1339 (2016)
273. Buschert R C *Bull. Am. Phys. Soc.* **10** 125 (1965)
274. Hart M *Proc. R. Soc. Lond. A* **309** 281 (1969)

275. Buschert R C et al. *J. Appl. Cryst.* **16** 599 (1983)
276. Ando M, Bailey D, Hart M *Acta Cryst. A* **34** 484 (1978)
277. Häusermann D, Hart M *J. Appl. Cryst.* **23** 63(1990)
278. Koval'chuk M V, Kov'ev E K, Pinsker Z G *Sov. Phys. Crystallogr.* **20** 81 (1975); *Kristallogr.* **20** 142 (1975)
279. Buschert R C et al. *Phys. Rev. B* **38** 5219 (1988)
280. Larson B C *J. Appl. Phys.* **45** 514 (1974)
281. Baker J F C et al. *Solid-State Electron.* **19** 331 (1976)
282. Cembali F et al. *J. Appl. Cryst.* **25** 424 (1992)
283. Kishino S *Adv. X-Ray Anal.* **16** 367 (1973)
284. Popovic S *J. Appl. Cryst.* **4** 240 (1971)
285. Fukumori T, Futagami K, Matsunaga K *Jpn. J. Appl. Phys.* **21** 1525 (1982)
286. Fukumori T, Futagami K *Jpn. J. Appl. Phys.* **27** 442 (1988)
287. Fukumori T et al. *J. Phys. Soc. Jpn.* **66** 1976 (1997)
288. Becker P, Scyfried P, Siegert H *Z. Phys. B* **48** 17 (1982)
289. Siegert H, Becker P, Seyfried P *Z. Phys. B* **56** 273 (1984)
290. Kubena J, Holý V *J. Appl. Cryst.* **21** 245 (1988)
291. Kessler E G et al. *J. Res. Natl. Inst. Stand. Technol.* **99** 1 (1994)
292. Martin J et al. *Metrologia* **35** 811 (1998)
293. Kessler E G et al. *IEEE Trans. Instrum. Meas.* **48** 221 (1999)
294. Mana G, Palmisano C, Zosi G *J. Appl. Cryst.* **37** 773 (2004)
295. Hanke M, Kessler E G *J. Phys. D* **38** A117 (2005)
296. Kessler E G et al. *J. Res. Natl. Inst. Stand. Technol.* **122** 1 (2017)
297. Bonse U et al. *Phys. Status Solidi A* **43** 487 (1977)
298. Massa E et al. *Metrologia* **48** S44 (2011)